European Journal of Medicinal Chemistry 146 (2018) 636–650

Contents lists available at ScienceDirect

European Journal of Medicinal Chemistry

journal homepage: http://www.elsevier.com/locate/ejmech

Research paper

Ridaifen-F conjugated with cell-penetrating peptides inhibits intracellular proteasome activities and induces drug-resistant cell death

Makoto Tanaka [a], Yunhao Zhu [a], Masafumi Shionyu [a], Nozomi Ota [b], Natsumi Shibata [b], Chihiro Watanabe [b], Akihito Mizusawa [b], Ryuzo Sasaki [a], Tamio Mizukami [a], Isamu Shiina [b, **], Makoto Hasegawa [a, *]

[a] Faculty of Bioscience, Nagahama Institute of Bio-Science and Technology, 1266 Tamura-cho, Nagahama, Shiga 526-0829, Japan
[b] Department of Applied Chemistry, Faculty of Science, Tokyo University of Science, 1-3 Kagurazaka, Shinjuku-ku, Tokyo 162-8601, Japan

ARTICLE INFO

Article history:
Received 27 October 2017
Received in revised form
27 December 2017
Accepted 15 January 2018
Available online 31 January 2018

Keywords:
Proteasome inhibitor
Tamoxifen derivative
Cell-penetrating peptide
Docking study

ABSTRACT

Ridaifen-F (RID-F) potently inhibits proteolytic activities of the 20S proteasome but poorly inhibits those of the 26S proteasome. Here, we report preparation of several conjugates in which various peptides are connected to RID-F. Conjugates with peptides consisting of seven amino acid residues significantly inhibited the 26S proteasome. Particularly, RID-F conjugated to an octaarginine peptide (R_8, a so-called cell-penetrating peptide) inhibited intracellular proteasome activities and induced cell death in drug-resistant KMS-11 myeloma cells. RID-F conjugated to hydrophobic peptides also inhibited the 26S proteasome but failed to induce cell death, suggesting poor penetration into cells. We infer that the R_8 peptide has dual functions: (1) rapid penetration of conjugates into the cell increases intracellular drug concentrations sufficient for exhibition of its effect, and (2) recognition of the conjugates by the 26S proteasome stimulates drug entry into the catalytic chamber. In the presence of ATPγS, RID-F conjugates containing R_8 inhibited the 26S proteasome more potently than in the presence of ATP, suggesting efficient entry of drugs into the catalytic chamber in a similar fashion to the substrate. Taken together with docking simulations of RID-F conjugate interactions with proteasome active sites, the second function of R_8 peptide is plausible. Thus, the conjugation of nonpeptidic proteasome inhibitors to a cell-penetrating peptide could represent a viable strategy for overcoming the drug-resistance of tumor cells.

1. Introduction

In eukaryotic cells, protein degradation by the ubiquitin-proteasome system plays a pivotal role in the regulation of various cellular processes including proliferation, differentiation, apoptosis, gene transcription, signal transduction, and quality control of nascent proteins [1]. The 26S proteasome, which is constitutively present in eukaryotic cells, comprises a barrel-shaped core particle (20S proteasome) and the 19S regulatory particles (RPs) capping one or both ends of the 20S proteasome barrel [2–4]. The 20S proteasome consists of seven α-subunits (α1–7) and seven β-subunits (β1–7) that form respective heptameric ring structures (α-ring and β-ring). Two α-rings and two β-rings are stacked in an αββα arrangement, generating the barrel-like structure of the 20S proteasome. The proteolytic active sites are located inside the barrel, where the β1, β2, and β5 subunits are responsible for protease activities with distinct substrate specificities: β1 for peptidylglutamyl peptide hydrolase (PGPH), β2 for trypsin-like (T-L), and β5 for chymotrypsin-like (CT-L) activities [5,6].

The 19S RPs regulate translocation of substrates into the 20S proteasome barrel. There are two types of 19S RP sub-complexes, known as the lid and the base, which contain different subunits with different functions. Deubiquitylation and unfolding of substrates are required prior to translocation of substrates into the catalytic chamber. The lid removes ubiquitin from poly-ubiquitinated substrates [7,8], while the base unfolds the globular domains of substrates [9,10]. One of the components in the base, a

* Corresponding author.
** Corresponding author.
E-mail addresses: shiina@rs.kagu.tus.ac.jp (I. Shiina), m_hasegawa@nagahama-i-bio.ac.jp (M. Hasegawa).

https://doi.org/10.1016/j.ejmech.2018.01.045
0223-5234/

heterohexameric ring with AAA-ATPase modules, plays a critical role in substrate translocation into the 20S proteasome barrel and substrate unfolding. ATP binding to the base opens the gate for substrates to be translocated into the barrel, and subsequent hydrolysis of the bound ATP is required for substrate unfolding mediated by reverse chaperone or unfoldase associated with AAA-ATPases.

Disruption of the ubiquitin-proteasome system causes accumulation of incompatible regulatory proteins that trigger an apoptotic cascade, eventually leading to growth arrest and cell death. In comparison with normal cells, tumor cells are generally more sensitive to the proapoptotic effects of proteasome inhibition [11]. This was ascertained in multiple myeloma cells whose growth strongly relies on the transcription factor NFκB [12,13]. Binding of IκB to NFκB in the cytoplasm prevents translocation of NFκB into the nucleus. Stress-induced phosphorylation of IκB results in proteasome-dependent degradation of IκB and thus NFκB activation. Inhibition of the proteasome likely represses myeloma cell growth by maintaining NFκB in an inactive state. Thus, proteasome inhibitors (PIs) have emerged as a new class of molecular-targeted anticancer drugs [14].

Several PIs are in clinical use as anticancer drugs [13,14]. One inhibitor, the peptide boronate bortezomib, is approved for the treatment of multiple myeloma and mantle cell lymphoma [15,16]. The toxic boronate pharmacophore, however, is associated with severe adverse effects, which is why an epoxomicin analog, tetrapeptide epoxyketone carfilzomib, was developed and approved [17]. More recently, another peptide, boronate ixazomib, which is available for oral uptake, has been approved for the treatment of multiple myeloma in combination with two other drugs, lenalidomide and dexamethazone, after first-line therapy [18]. In addition to the treatment of hematological malignancies, PIs have been proposed as promising drug candidates for solid tumors, inflammation, immune diseases, ischemic stroke, and tuberculosis [19]. This situation encourages the development of new types of PIs with improved efficacy and fewer adverse effects [20].

To find new noncovalent and nonpeptidic PIs, we previously examined proteasome inhibition using a series of tamoxifen derivatives and found that ridaifen (RID)-A, -B, -D, and -F inhibited protease activities of the 20S proteasome [21]. RID-F (**1**) was the most potent inhibitor of the three different enzymatic activities. However, subsequent investigation indicated that RID-F derivatives were not effective against multidrug-resistant human multiple myeloma cells (KMS-11). Drug resistance can be caused by poor drug uptake, active excretion, intracellular degradation or modification, concentration of drugs into a specific subcellular compartment, and mutations that render target proteins insensitive to drugs. Although it is difficult to identify the mechanisms that give rise to drug resistance in individual cells, it is likely that poor drug uptake or active excretion is a prevalent mechanism, and therefore modification of drugs to improve uptake is a promising strategy.

Several proteins, such as Tat protein from human immunodeficiency virus-1 (HIV-1), can spontaneously penetrate cells [22]. The minimal domain needed for penetration was defined as a short sequence of 10–16 amino acids, termed a "cell-penetrating peptide" (CPP) [23]. Native Tat peptide is composed of several cationic amino acids, including six arginine and two lysine residues. Furthermore, the cationic peptide, octaarginine (R_8), can promote cellular uptake of conjugated compounds. Although several hypotheses explaining how these peptides penetrate cells have been presented [24,25], the underlying mechanism still remains unclear. Nevertheless, CPPs can be used for the translocation of peptides, proteins, ribonucleic acids, oligonucleotide mimics, and nanoparticles through cell membranes. Since CPPs can also transport nonpermeable drugs into living cells, they are of considerable pharmaceutical interest. Studies of conjugating CPPs to several drugs, including methotrexate [26], doxorubicin [27–31], and organometal conjugates [32–34], have been reported. Tat peptide conjugated to doxorubicin significantly increases the intracellular concentration of the drug in both drug-sensitive and drug-resistant cell lines [29].

In this study, we prepared conjugates of RID-F and various peptides, including oligo-arginines, and compared their inhibitory potency on the protease activities of the 20S and 26S proteasomes. Notably, RID-F conjugates containing R_8 showed a strong inhibitory potency toward 26S proteasome activity in comparison with that of free RID-F. Furthermore, these RID-F conjugates overcame KMS-11 cell drug resistance, rapidly inducing cell death. We confirmed that these conjugates inhibited proteolytic activities of the intracellular proteasome. These results suggest that conjugation of nonpeptidic PIs with CPPs is a viable strategy to overcome tumor-cell drug resistance.

2. Results

2.1. Synthetic procedures

We previously presented the synthesis and characterization of a novel tamoxifen derivative, RID-F (**1**), which inhibits 20S proteasome activity. RID-F was synthesized chemically as described in previous reports [21,35,36]. RID-F derivatives (RID-F-COOH (**15**) and RID-F-CH_2NH_2 (**19**)) were prepared by the Mukaiyama reductive coupling reaction [37,38], as shown in Schemes 1 and 2. The 1,3-phenylenedimethanol (**2**) was first mono-protected with a *p*-methoxybenzyl group and the following two-carbon elongation of the intermediate **4** to afford 1-(3′-((*p*-methoxybenzyloxy)methyl) phenyl)propan-1-one (**6**). Then, **6** was treated with an excess amount of 4,4′-dihydroxybenzophenone (**7**) in the presence of the low-valent titanium species generated from titanium(IV) chloride with zinc powder to afford the desired cross-coupling product **8** in 52% yield. The phenol moieties in **8** were temporarily protected as *tert*-butyldimethylsilyl (TBS) groups and finally transformed into the corresponding aminoethyl ethers by alkylation of **14**. Fortunately, the benzyl protective group in the tetra-substituted olefin **14** was simultaneously cleaved in the alkylation reaction under nucleophilic conditions to provide the desired RID-F derivative **15** including the free carboxylic acid part.

Next, RID-F derivative **19**, including the free primary amine part, was also synthesized using a similar procedure as described in Scheme 2. Aminoethyl groups were introduced into the bisphenol **17** in 77% yield, and the desired free primary amine **19** was successfully prepared from benzyl oxime **18** by reduction using lithium aluminum hydride in 77% yield.

Peptides and the RID-F derivatives were linked at the N- or C-terminus of the peptides by amide bond formation (Scheme 3). In the peptides used for the conjugation, the opposite terminus to the site linked with the RID-F derivatives was blocked by modification with an amide (C-terminus) or acetyl group (N-terminus). The chemical structures of representative compounds, RID-F (**1**), RID-F-GR_8 (**27**), and R_8G-RID-F (**31**), are depicted in Fig. 1. The purities of all the conjugates were confirmed by analytical reversed-phase high-performance liquid chromatography (RP-HPLC) analysis and matrix-assisted laser desorption/ionization-time of flight (MALDI-TOF) mass measurements, and were above 95% (Supplementary Fig. 4). The *m*/*z* values of these compounds were observed to be identical with the theoretical values (Supplementary Table 1).

2.2. Proteasome inhibition by RID-F-CPP conjugates

To assess the potency of proteasome inhibition of RID-F (**1**) and

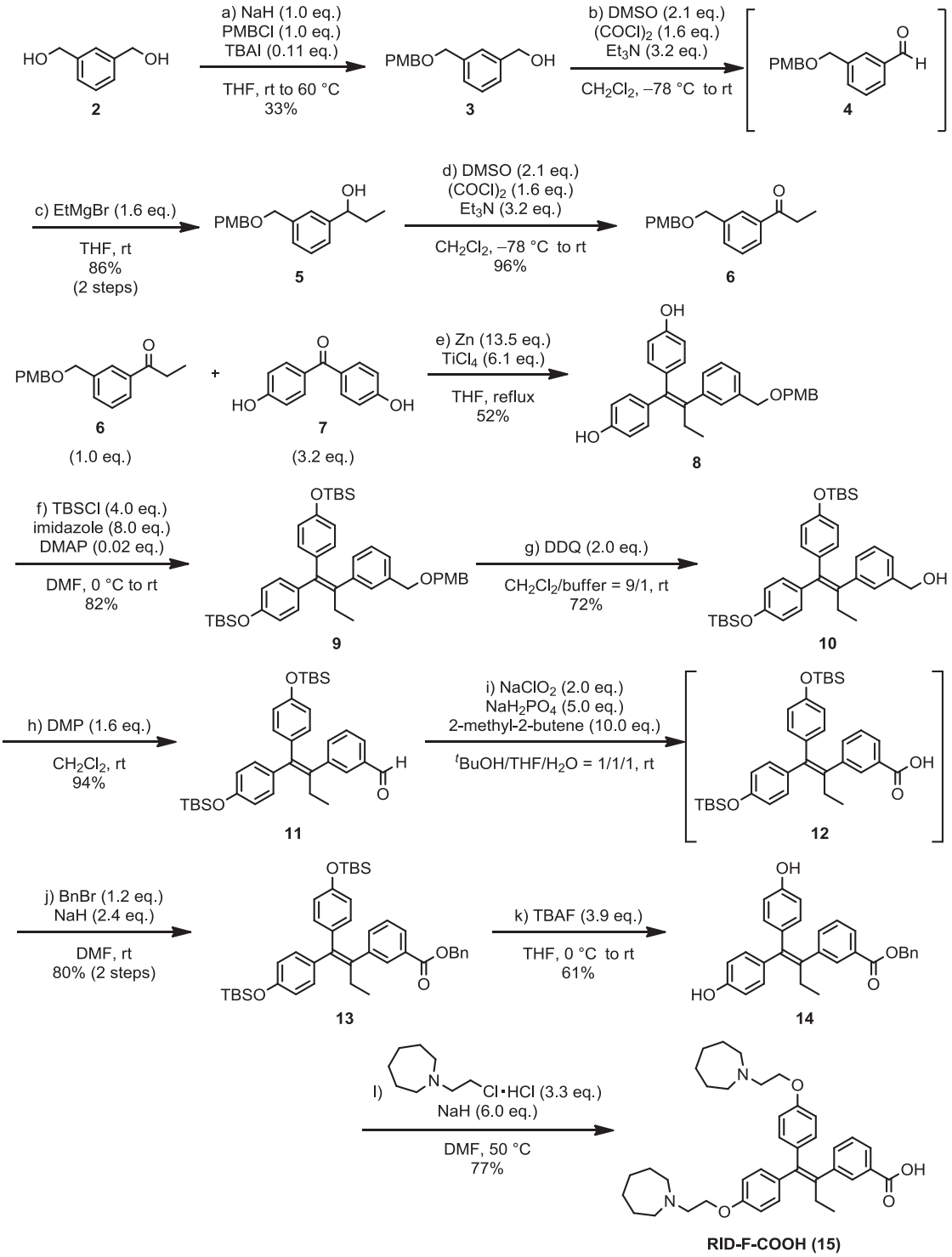

Reagents and conditions: a) NaH (1.0 eq.), PMBCl (1.0 eq.), TBAI (0.11 eq.), THF, rt to 60 °C, 33%; b) DMSO (2.1 eq.), $(COCl)_2$ (1.6 eq.), Et_3N (3.2 eq.), CH_2Cl_2, –78 °C to rt; c) EtMgBr (1.6 eq.), THF, rt, 86% (2 steps); d) DMSO (2.1 eq.), $(COCl)_2$ (1.6 eq.), Et_3N (3.2 eq.), CH_2Cl_2, –78 °C to rt, 96%; e) Zn (13.5 eq.), $TiCl_4$ (6.1 eq.), THF, reflux, 52%; f) TBSCl (4.0 eq.), imidazole (8.0 eq.), DMAP (0.02 eq.), DMF, 0 °C to rt, 82%; g) DDQ (2.0 eq.), CH_2Cl_2/buffer = 9/1, rt, 72%; h) DMP (1.6 eq.), CH_2Cl_2, rt, 94%; i) $NaClO_2$ (2.0 eq.), NaH_2PO_4 (5.0 eq.), 2-methyl-2-butene (10.0 eq.), $^tBuOH/THF/H_2O$ = 1/1/1, rt; j) BnBr (1.2 eq.), NaH (2.4 eq.), DMF, rt, 80% (2 steps); k) TBAF (3.9 eq.), THF, 0 °C to rt, 61%; l) 1-(2-chloroethy)azepane hydrochloride (3.3 eq.), NaH (6.0 eq.), DMF, 50 °C, 77%.

Scheme 1. Synthesis of RID-F-COOH (**15**).

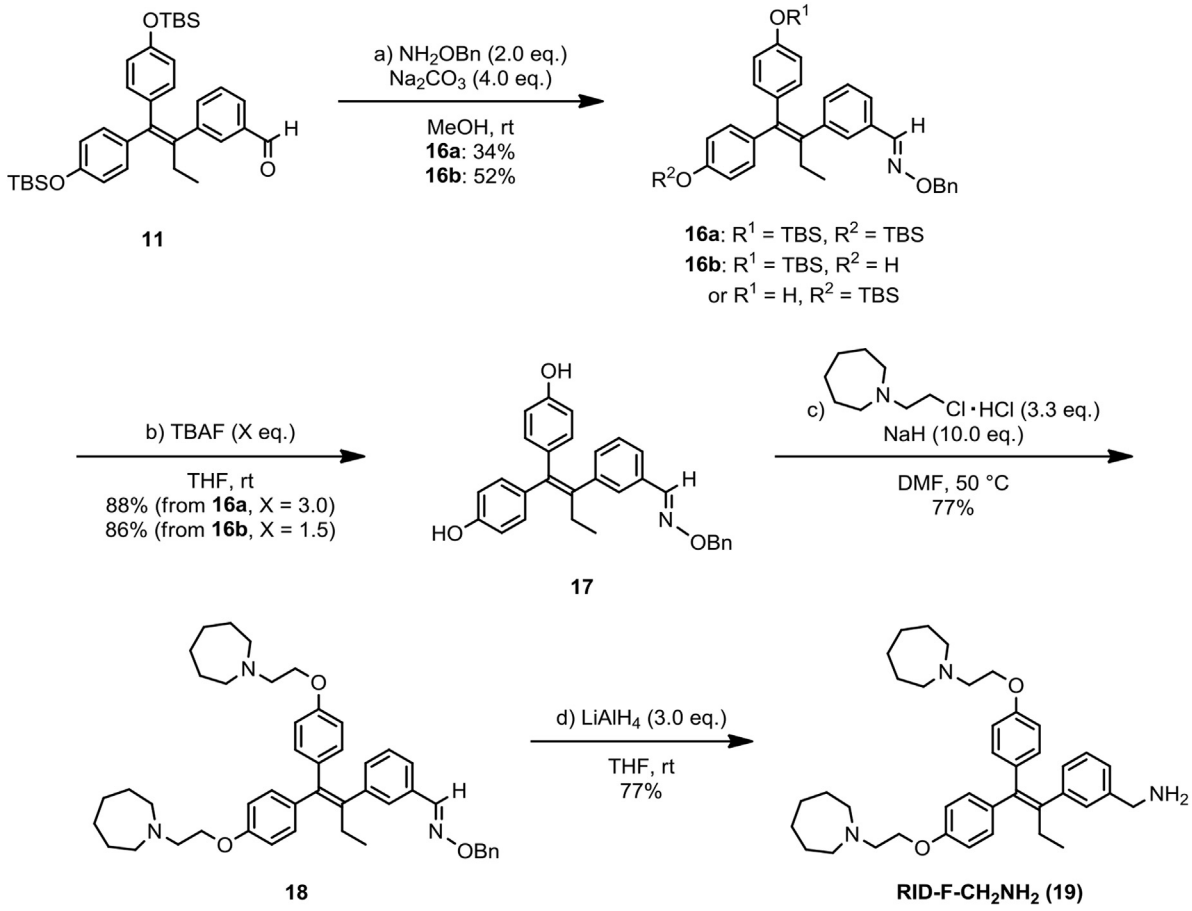

Reagents and conditions: a) NH_2OBn (2.0 eq.), Na_2CO_3 (4.0 eq.), MeOH, rt, **16a**: 34%, **16b**: 52%; b) TBAF (X eq.), THF, rt, 88% (from **16a**, X = 3.0), 86% (from **16b**, X = 1.5); c) 1-(2-chloroethyl)azepane hydrochloride (3.3 eq.), NaH (10.0 eq.), DMF, 50 °C, 77%; d) $LiAlH_4$ (3.0 eq.), THF, rt, 77%.

Scheme 2. Synthesis of RID-F-CH_2NH_2 (**19**).

its CPP conjugates (RID-F-GR_8 (**27**) and R_8G-RID-F (**31**)), three proteolytic activities (PGPH, T-L, and CT-L) were examined with an enzymatic kinetics assay using fluorogenic substrates. To promote the passage of peptidyl substrates to the catalytic chamber, sodium dodecyl sulfate (SDS) was present at 0.03% for assaying the 20S proteasome and ATP was present at 1 mM for assaying the 26S proteasome. The inhibition curve of each compound is depicted in Supplementary Fig. 1. Their IC_{50} values are summarized in Table 1.

Free RID-F inhibited PGPH and CT-L activities of the 20S proteasome, but did not inhibit the three activities of the 26S proteasome. RID-F-GR_8 (**27**) and R_8G-RID-F (**31**) inhibited T-L activity of the 20S proteasome. Although these two conjugates containing R_8 did not inhibit the CT-L activity of the 20S proteasome, they strongly inhibited the CT-L activity of the 26S proteasome. Thus, the inhibitory potency and specificity of the RID-F conjugates alter depending on the proteasome type (20S and 26S). Such alterations are also found with conventional inhibitors such as bortezomib, vinblastine, and lactacystin. The gate of the 20S proteasome chamber is normally closed so that substrates and PIs cannot enter the chamber freely [39]. The presence of SDS enables ingress of these substrates and inhibitors into the chamber [40]. On the other hand, the AAA ring of the 19S RP in the 26S proteasome forms a channel through which these substances enter the 20S chamber in an ATP-dependent manner. Alterations in the potency and specificity of PIs are due to structural differences in the two types of proteasomes; however, structural information alone is insufficient for delineating the molecular mechanisms underlying these alterations. Regardless of the mechanism, the marked inhibition of the CT-L activity of the 26S proteasome by RID-F conjugates containing R_8 encouraged further study.

Basic peptides with 4–10 R residues inhibit CT-L and PGPH activities of the 20S proteasome at submicromolar levels [41]. However, free GR_8 (C-terminal amidated) or R_8G peptides (N-terminal acetylated) did not inhibit the protease activities of the 26S proteasome (Table 1), indicating that RID-F-CPP conjugate-mediated inhibition of the 26S proteasome was not attributable to the basic peptides in the conjugates.

ATP is typically added for assaying the 26S proteasome. It is of interest to examine whether ATP hydrolysis is required for degradation of small substrates (in our assay) by the 26S proteasome. ATPγS, which is hydrolyzed at a much slower rate than ATP, was used to address this question. As shown in Fig. 2A, 26S proteasome CT-L activity was higher in the presence of ATPγS than ATP, while there was no effect on 20S proteasome CT-L activity. Thus, ATP hydrolysis is not required for 26S proteasome CT-L activity for small substrates. Next, the effect of ATPγS on the inhibitory potency of RID-F conjugates was examined. Interestingly, in the presence of ATPγS, both RID-F-GR_8 (**27**) and R_8G-RID-F (**31**) showed stronger

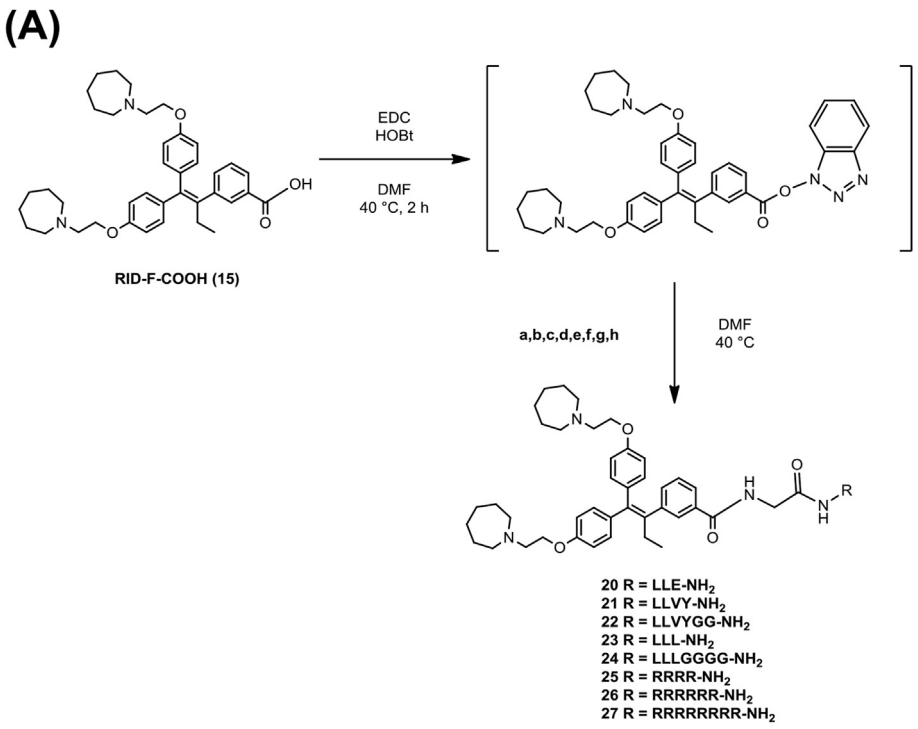

Reagents and conditions:
(a) H-GLLE-NH_2 (3.0 eq.), DMF, 40 °C, 6 h, (b) H-GLLVY-NH_2 (2.0 eq.), DMF, 40 °C, 5 h,
(c) H-GLLVYGG-NH_2 (2.0 eq.), DMF, 40 °C, 6 h, (d) H-GLLL-NH_2 (2.0 eq.), DMF, 40 °C, 6 h,
(e) H-GLLLGGGG-NH_2 (2.0 eq.), DMF, 40 °C, 6 h, (f) H-GRRRR-NH_2 (2.0 eq.), DMF, 40 °C, 4 h,
(g) H-GRRRRRR-NH_2 (2.0 eq.), DMF, 40 °C, 4 h, (h) H-GRRRRRRRR-NH_2 (2.0 eq.), DMF, 40 °C, 4 h.

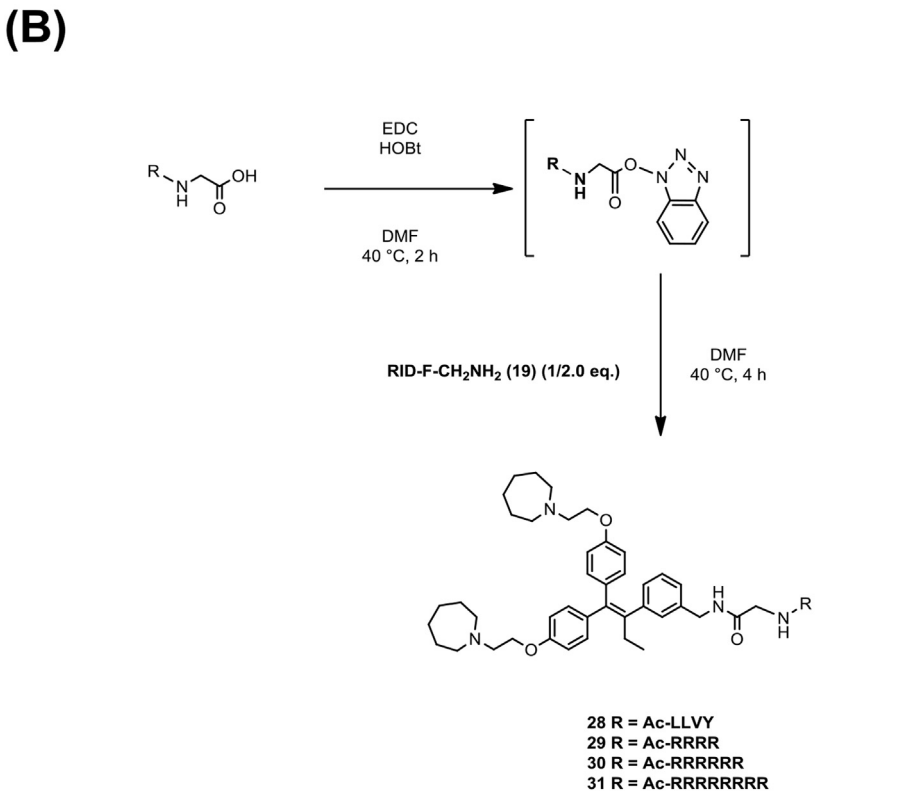

Scheme 3. Conjugation of RID-F derivatives and peptides at the N-terminus (A) or C-terminus (B).

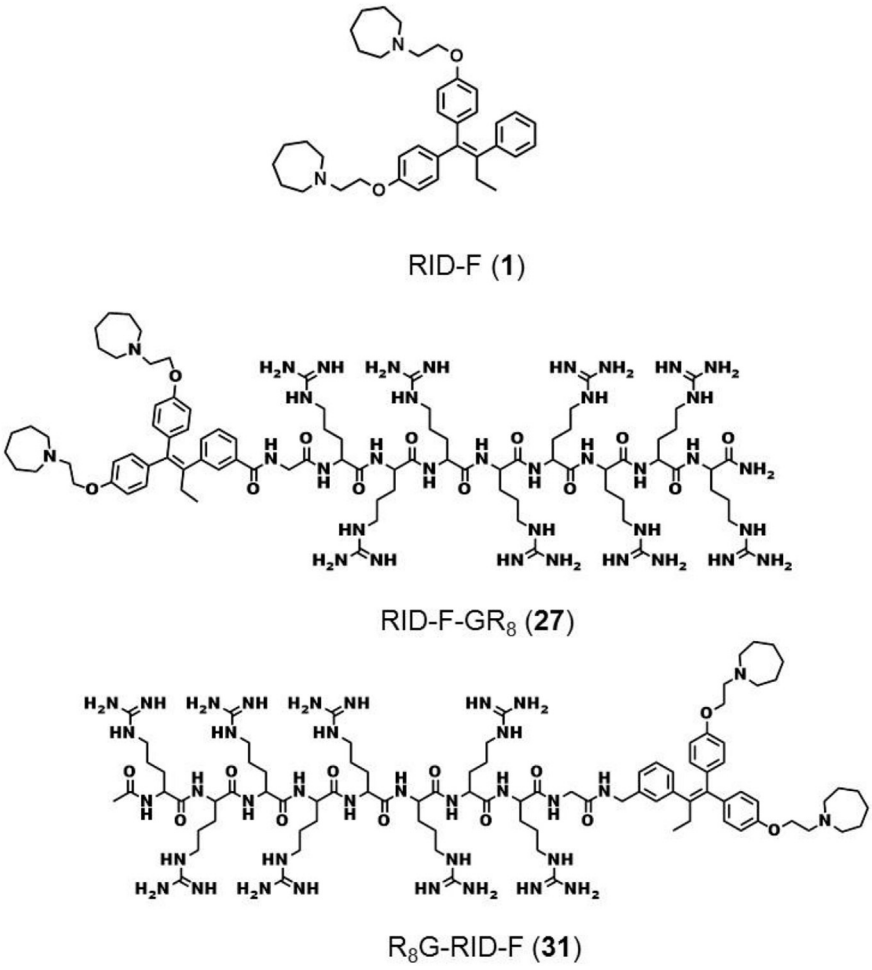

Fig. 1. Structure of RID-F and CPP conjugates.

Table 1
IC_{50} values of CPP-conjugated RID-F against the human 20S and 26S proteasome.

	20S IC_{50} (μM)			26S IC_{50} (μM)		
	β1 (PGPH)	β2 (T-L)	β5 (CT-L)	β1 (PGPH)	β2 (T-L)	β5 (CT-L)
RID-F (**1**)	0.72 ± 0.10	>100	1.02 ± 0.02	>100	>100	>100
RID-F-GR_8 (**27**)	>50	1.2 ± 0.3	>50	>50	45 ± 4	5.5 ± 0.2
R_8G-RID-F (**31**)	>40	3.5 ± 0.8	>40	>40	>40	9.4 ± 1.2
H-GR_8-NH_2	>8	>8	>8	>40	>40	>40
Ac-R_8G-OH	>8	>8	>8	>40	>40	>40
Bortezomib	0.7 ± 0.08	1.93 ± 0.29	0.0005 ± 0.0004	0.019 ± 0.005	>40	2.1 ± 0.5
Vinblastine	4.28 ± 0.54	4.90 ± 0.34	4.58 ± 0.43	>40	14.50 ± 2.29	>40
Lactacystin	>8.0	3.25 ± 0.54	0.16 ± 0.01	>40	>40	4.96 ± 0.17

Abbreviations: IC_{50}, half-maximum inhibitory concentration; CT-L, chymotrypsin-like activity; T-L, trypsin-like activity; PGPH, peptidylglutamyl peptide hydrolase activity. Data are given as means ± SD (n = 3).

inhibition than in the presence of ATP; IC_{50} values of RID-F-GR_8 and R_8G-RID-F against 26S proteasome CT-L activity significantly shifted to lower values of 2.4 μM and 6.0 μM, respectively (Fig. 2B and C). Free RID-F did not inhibit CT-L activity in the presence of either ATPγS or ATP (Fig. 2D).

2.3. Proteasome inhibition by RID-F conjugates containing various peptides

We evaluated how the sequence and length of peptides conjugated to RID-F affected the inhibitory potency for proteolytic activities of the 20S and 26S proteasomes. The potency of nine types of RID-F-peptide conjugates, including basic and hydrophobic residues, was examined. Inhibition curves are shown in Supplementary Fig. 2. The IC_{50} values are summarized in Table 2.

When the 20S proteasome was examined, RID-F-peptide conjugates with different lengths of arginine repeats, RID-F-GR_4 (**25**), RID-F-GR_6 (**26**), R_4G-RID-F (**29**), and R_6G-RID-F (**30**), showed significant inhibition of T-L activity. From their IC_{50} values, the N-terminal peptide conjugates, RID-F-GR_4 (**25**) and RID-F-GR_6 (**26**), were approximately 10 times more potent than C-terminal peptide conjugates, R_4G-RID-F (**29**) and R_6G-RID-F (**30**). Three hydrophobic

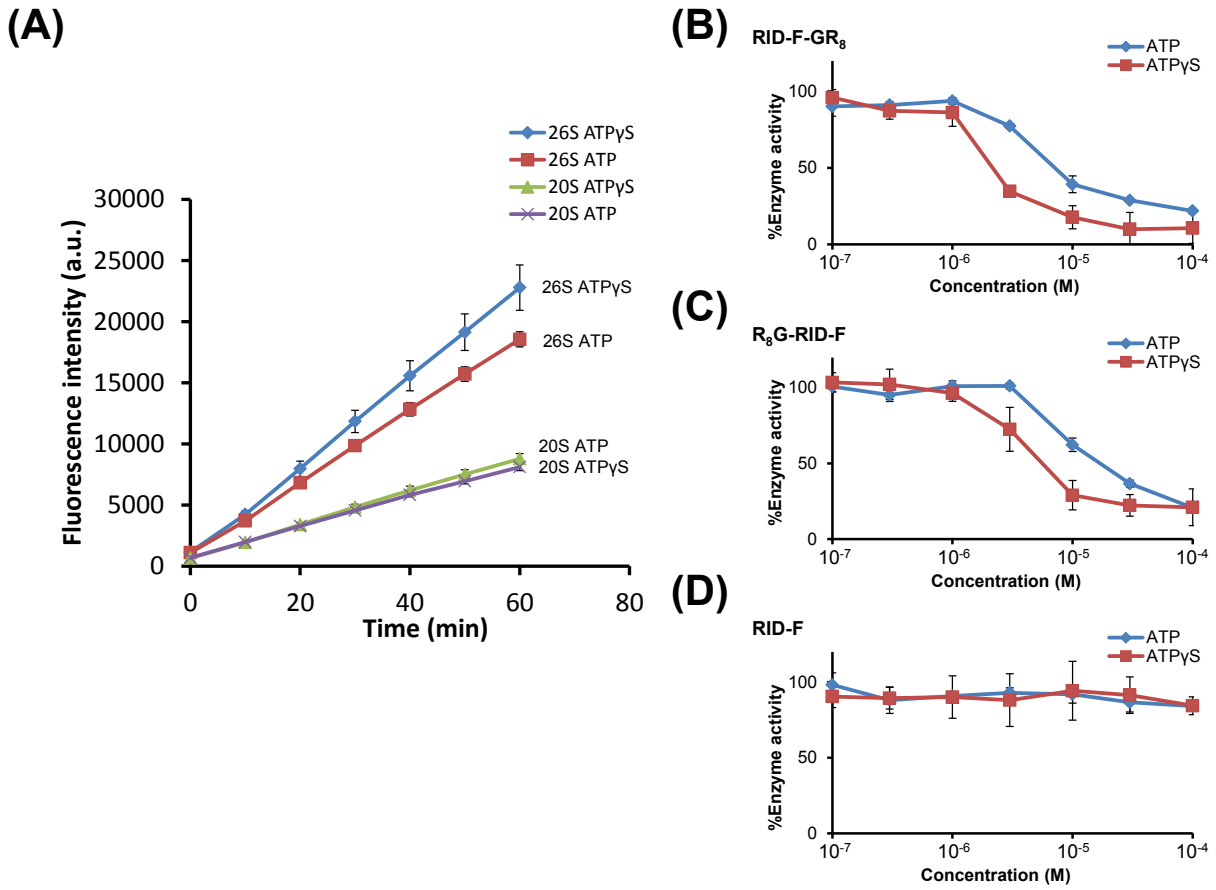

Fig. 2. (A) Kinetics of fluorogenic substrate degradation in the presence of ATP or ATPγS. Values are means ± SEM of three independent experiments. (B–D) Inhibition of the 26S proteasome in the presence of ATP (blue circles) or ATPγS (red squares). Results are means ± SEM of three independent experiments. (For interpretation of the references to color in this figure legend, the reader is referred to the Web version of this article.)

Table 2
Inhibition of the human 20S and 26S proteasome by peptide-conjugated RID-F.

	20S IC_{50} (μM)			26S IC_{50} (μM)		
	β1 (PGPH)	β2 (T-L)	β5 (CT-L)	β1 (PGPH)	β2 (T-L)	β5 (CT-L)
RID-F-GR_4 (**25**)	>8	0.35 ± 0.06	>8	>40	>40	>40
RID-F-GR_6 (**26**)	>8	0.20 ± 0.10	>8	>40	>40	>40
R_4G-RID-F (**29**)	>8	3.7 ± 0.3	>8	>40	>40	>40
R_6G-RID-F (**30**)	3.3 ± 1.0	3.2 ± 0.2	>8	>40	>40	>40
RID-F-GLLE (**20**)	4.5 ± 0.3	>8	6.1 ± 1.1	>40	>40	24 ± 1
RID-F-GLLVY (**21**)	0.89 ± 0.08	8.9 ± 1.2	0.89 ± 0.09	33 ± 9	>40	26 ± 3
LLVYG-RID-F (**28**)	0.28 ± 0.01	>8	0.37 ± 0.14	>40	>40	>40
RID-F-GLLVYGG (**22**)	0.99 ± 0.04	6.9 ± 0.8	0.89 ± 0.16	22 ± 7	>40	9.1 ± 1.0
RID-F-GLLLGGGG (**24**)	0.89 ± 0.08	3.8 ± 0.6	1.1 ± 0.2	17 ± 7	32 ± 3	5.0 ± 0.9

Abbreviations: IC_{50}, half-maximum inhibitory concentration; CT-L, chymotrypsin-like activity; T-L, trypsin-like activity; PGPH, peptidylglutamyl peptide hydrolase activity. Data are given as means ± SD (n = 3). Inhibition of the 20S core particle and 26S proteasome was evaluated in concentration ranges of 0.5–8 μM and 0.1–40 μM, respectively.

peptide conjugates, RID-F-GLLE (**20**), RID-F-GLLVY (**21**), and LLVYG-RID-F (**28**), strongly inhibited CT-L and PGPH activities, but these activities were insensitive to RID-F conjugates that contained R. Thus, the chemical properties of the peptides present in the RID-F conjugate influence the inhibitory specificity for the 20S proteasome; conjugates that contain basic peptides favorably inhibit T-L activity, and those that contain hydrophobic peptides do so for CT-L and PGPH activities. Notably, all of the conjugates that contained less than six amino acids showed minimal inhibition of the 26S proteasome. However, conjugates with longer peptides, such as RID-F-GLLVYGG (**22**) and RID-F-GLLLGGGG (**24**), showed significant inhibition of the 26S proteasome. Taken together with the results of RID-F-GR_8 (**27**) and R_8G-RID-F (**31**), conjugation with a peptide consisting of seven or more amino acid residues was required for significant inhibition of 26S proteasome activities. This requirement suggests that the peptide portion of the RID-F conjugate interacts with the 26S proteasome, although the site of interaction remains to be studied.

2.4. Cellular proteasome inhibition by RID-F conjugates and their cytotoxic effect on multidrug-resistant myeloma cells

Since RID-F CPP conjugates, but not free RID-F, inhibited the 26S proteasome (see Table 1), we examined the effects of the conjugate

on the cellular proteasome using two cell lines, multidrug-resistant human multiple myeloma cells (KMS-11) and drug-sensitive multiple myeloma cells (RPMI8226), and a Proteasome-Glo™ Assay kit (Promega Co.), which enables the direct measurement of intracellular proteasome activities in cultured cells [42]. Multidrug-resistance of KMS-11 cells was confirmed by using cisplatin (Table 3). Inhibition of three proteasome activities by RID-F (**1**), RID-F-GR_8 (**27**), and R_8G-RID-F (**31**) was measured in the presence of various concentrations of the conjugates, and IC_{50} values were calculated from inhibition curves (Supplementary Fig. 3). Free RID-F did not inhibit CT-L, PGPH, and T-L activities of the intracellular proteasome in KMS-11 cells, whereas R_8G-RID-F and RID-F-GR_8 significantly inhibited all three activities to a similar extent; IC_{50} values were 2–8 μM (Table 3). On the other hand, RID-F-GR_8, and R_8G-RID-F comparably inhibited CT-L and PGPH activities in RPMI8226 cells, but RID-F inhibited only CT-L activity with slightly lower potency.

Similarly, cell survival rates were measured by quantifying ATP levels to determine Cyt_{50} values for each conjugate. As shown in Table 3, RID-F-GR_8 and R_8G-RID-F induced cell death of KMS-11 and RPMI8226 cells with similar potency (Cyt_{50} = 4–8 μM). Remarkably, these RID-F conjugates exerted their inhibitory effects on the proteasome and cell survival with similar potency. Fig. 3 shows time-dependent death of KMS-11 cells cultured in the presence of 10 μM of each compound. Viable cell counts were markedly decreased upon culture for 6 h in the presence of RID-F-GR_8 or R_8G-RID-F, whereas the effect of free RID-F was undetectable. On the other hand, RID-F, RID-F-GR_8, and R_8G-RID-F induced comparable levels of cell death in RPMI8226 cells.

2.5. Molecular docking simulations

To determine how RID-F-peptide conjugates bind the proteasome to exhibit their inhibitory effect, docking studies using AutoDock Vina [43] were conducted. To date, several three-dimensional (3D) structures of the human proteasome have been reported. We used structural data of the human 20S proteasome complexed with dihydroeponemycin (Protein Data Bank ID: 5lf1 [44]). Estimated binding modes of RID-F-GR (Fig. 4A) and RG-RID-F (Fig. 4B) were obtained from clusters composed of 23 and 26 docking poses, respectively (see Experimental Protocols for details). The estimated binding affinities of RID-F-GR and RG-RID-F were −9.1 (the second highest value in 100 docking poses) and −9.5 kcal/mol (the highest value in 100 docking poses), respectively. In the estimated binding mode of RID-F-GR, the guanidyl group of the Arg residue in RID-F-GR entered the S1 pocket [19] of the β5 subunit, and the two homopiperidine rings interacted with the β6 subunit (Fig. 4A). For RG-RID-F, two homopiperidine rings also interacted with similar sites in the β6 subunit to the ones used for RID-F-GR binding, but the amino group in the main chain of Arg entered the S1 pocket instead of the guanidyl group (Fig. 4B). In the previous study, it was suggested that the vinyl benzene group of RID-F or the homopiperidine ring of some RID-F derivatives is important for interacting with the S1 pocket of the β1 subunit [21]. The estimated binding modes of RID-F-GR and RG-RID-F in the present study suggest that a different manner of homopiperidine ring usage is important for interactions between CPP-conjugated RID-F and the proteasome. Moreover, although the main chain direction of the amino acid moiety was different between RID-F-GR and RG-RID-F, the estimated binding modes were somewhat similar between each other; the substrate-binding cleft composed of the S1 to S5 pockets was almost buried due to the interactions of the amino acid moiety with the S1 pocket and the RID-F moiety with the β6 subunit. This binding mode prevented substrates from interacting with the binding cleft widely and mediated the inhibitory effect of CPP-conjugated RID-F.

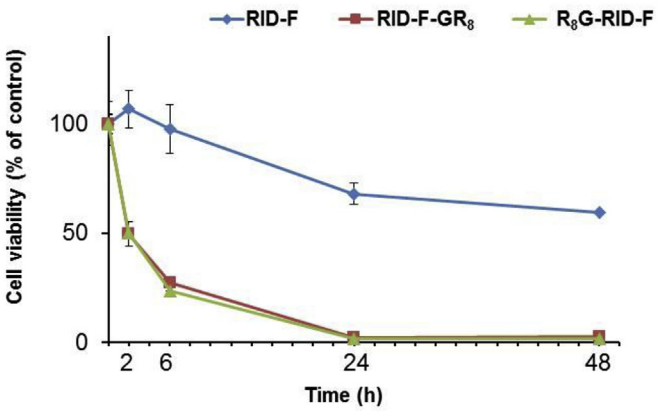

Fig. 3. Time dependency of KMS-11 cell viability in the presence of RID-F (blue circles), RID-F-GR_8 (red squares), and R_8G-RID-F (green triangles) (10 μM) determined with an ATP assay. The viability of mock-treated cells served as a standard (100%). Results are means ± SEM of three independent experiments. (For interpretation of the references to color in this figure legend, the reader is referred to the Web version of this article.)

3. Discussion

RID-F, a novel tamoxifen derivative, inhibited the human 20S proteasome [21]. Our subsequent studies of the 26S proteasome, however, showed that RID-F poorly inhibited its proteolytic activities. Furthermore, RID-F failed to kill KMS-11 cells, a multidrug-resistant human myeloma cell line. To overcome these drawbacks of RID-F, we prepared various RID-F-peptide conjugates. This concept was based on the findings of CPPs (see Introduction). In this paper, we hypothesized the dual functions of peptide moieties in RID-F-peptide conjugates with respect to inhibition of the cellular

Table 3
Proteasome inhibition and cytotoxicity in KMS-11 cells and RPMI8226 cells.

	KMS-11				RPMI8226			
	IC_{50} (μM)			Cyt_{50} (μM)	IC_{50} (μM)			Cyt_{50} (μM)
	CT-L	PGPH	T-L		CT-L	PGPH	T-L	
RID-F (**1**)	N.D.	N.D.	N.D.	N.D.	11.0 ± 0.8	N.D.	N.D.	3.6 ± 0.6
RID-F-GR_8 (**27**)	6.3 ± 1.6	4.8 ± 0.8	8.0 ± 1.8	7.2 ± 1.0	5.7 ± 0.2	6.6 ± 0.2	N.D.	4.3 ± 0.3
R_8G-RID-F (**31**)	2.1 ± 0.7	2.8 ± 1.2	4.1 ± 0.3	4.5 ± 0.1	2.1 ± 0.6	3.1 ± 0.1	N.D.	2.7 ± 0.4
H-GR_8-NH_2	N.D.	N.D.	N.D.	N.D.	N.D.	N.D.	N.D.	N.D.
Ac-R_8G-OH	N.D.	N.D.	N.D.	N.D.	N.D.	N.D.	N.D.	N.D.
cisplatin	–	–	–	N.D.	–	–	–	1.18 ± 0.88

Abbreviations: N.D., not detected; IC_{50}, half-maximum inhibitory concentration; CT-L, chymotrypsin-like activity; T-L, trypsin-like activity; PGPH, peptidylglutamyl peptide hydrolase activity; -, not determined. Data are given as means ± SD (n = 3).

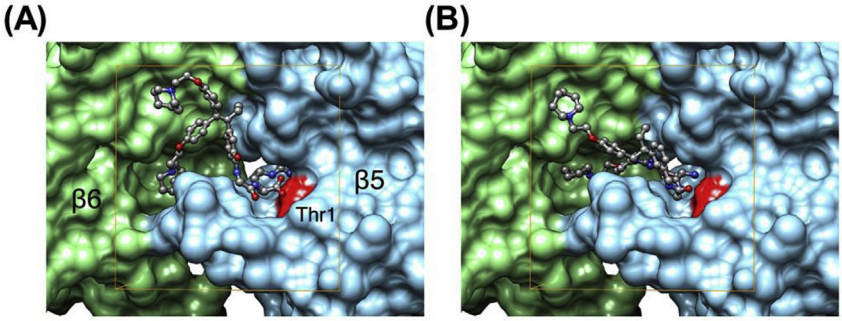

Fig. 4. Estimated binding modes of RID-F-GR (A) and RG-RID-F (B) with the CT-L site of the human proteasome. The β5 and β6 subunits of the human proteasome are shown as a surface model colored in cyan and green, respectively. Thr1 of the β5 subunit is colored in red. The docked RID-F-GR and RG-RID-F are shown as a ball-and-stick model with carbon, nitrogen, and oxygen atoms in gray, blue, and red, respectively. Orange lines indicate the boundaries of the docking grid box for the AutoDock Vina run. All images were generated using UCSF Chimera 1.11.2 [56]. (For interpretation of the references to color in this figure legend, the reader is referred to the Web version of this article.)

proteasome. Firstly, peptide moieties are recognized by the proteasome as substrates, thereby facilitating the entry of conjugates into the catalytic chamber. Secondly, peptide moieties promote penetration of conjugates into cells, thereby increasing intracellular concentrations of RID-F to levels sufficient for proteasome inhibition. We found that RID-F conjugates containing R_8 inhibited not only the 26S proteasome but also the intracellular proteasome in KMS-11 cells. Furthermore, these compounds induced cell death. Interestingly, although these conjugates inhibited 26S proteasome CT-L activity only, they inhibited all three proteolytic activities in KMS-11 cells. The reason is unclear, but may involve unknown intracellular factor(s) that are missing in the isolated 26S proteasome.

The inhibitory potencies of RID-F-peptide conjugates against the 26S proteasome were dependent on the lengths and chemical properties of the peptides. Peptides consisting of at least seven amino acids were necessary for inhibition. Notably, hydrophobic peptides inhibited 26S CT-L activity with potencies comparable to those of R8. However, RID-F conjugates containing hydrophobic peptides did not influence cell survival (data not shown), suggesting that these conjugates do not enter the cell efficiently. Nevertheless, this is a useful finding to be taken into consideration for further improvement of RID-F conjugates.

Our experimental results with the 26S proteasome and ATPγS clearly indicate that 19S RPs are important for substrate entry into the CT-L active site, although ATP hydrolysis is not required. Instead, ATP hydrolysis may impede entry, because higher CT-L activity was seen in the presence of ATPγS than ATP. ATP hydrolysis would be required for unfolding of globular domains of large proteins before degradation. This is consistent with cryo-electron microscopic analyses of the 26S proteasome in the presence of ATPγS [39,45–47]; 26S proteasomal degradation of peptides and unfolded proteins requires ATP binding but not ATP hydrolysis. The presence of ATPγS instead of ATP may retain the 19S RP in an active conformation, opening the substrate entry gate for a prolonged time.

Unexpectedly, RID-F-GR_8 and R_8G-RID-F showed higher inhibition of 26S CT-L activity in the presence of ATPγS than ATP. At present, the precise reason is unclear, but it is plausible that entry of these compounds into the 20S chamber is stimulated in a similar fashion to that of the substrate, and somehow, they are accessible to the CT-L active site with high efficiency. Gibbs free energy changes in our molecular docking simulations indicated that RID-F-GR and RG-RID-F preferably bind the CT-L active site (data not shown).

Previous reports indicate that KMS-11 cells are resistant to several anticancer drugs [48] via overexpression of PDZK1 protein, which interacts with a multidrug resistance-associated protein MRP2 [49,50]. MRP2 is an efflux transporter, and PDZK1 mediates subcellular localization of target proteins (localization of MRP2 into the plasma membrane in this case). In our experiments, KMS-11 cells were not sensitive to RID-F and cisplatin, in contrast to RPMI8226 cells, which were. This suggests that KMS-11 cells possess the multidrug resistance previously proposed [48]. RID-F-GR_8 (**27**) and R_8G-RID-F (**31**) not only inhibited proteasomal activity in KMS-11 cells but also rapidly induced cell death. Taken together with the 26S proteasome data, R_8 peptide in the RID-F conjugates appears to have dual functions: stimulation of drug entry into the proteolytic chamber and stimulation of cellular uptake. Furthermore, R_8 may contribute to increased drug access to the CT-L active site. The presence of 1 μM of the RID-F conjugates, however, was poorly cytotoxic against KMS-11 cells, indicating that further structural improvement of the RID-F conjugates is required.

Our results collectively suggest the proposed mechanism in Fig. 5. Structural properties of RID-F (**1**) suggest that it can diffuse efficiently across the cell membrane. RID-F may act on the 20S form free from the 19S RPs, but does not significantly inhibit the major intracellular form, the 26S proteasome. Furthermore, RID-F (**1**) may be readily exported from cells, thus leading to poor efficacy against KMS-11 cells. RID-F-GR_8 (**27**) and R_8G-RID-F (**31**) are rapidly taken up by cells and efficiently translocated into the 26S proteasome. Within the proteasome proteolytic chamber, the peptide moiety may be cleaved, and RID-F conjugated to one or two amino acids mainly binds to the CT-L site (see Fig. 4). With the rapid increase in the number of CPP studies, drug delivery systems using CPPs that target tumor cells with high potency will likely become available [23,51]. However, for CPPs to be effective *in vivo*, it will be necessary to develop strategies that prevent cleavage of the conjugated peptides by blood proteases. This could be achieved by chemically modifying the peptide structures by, for example, macrocyclization, or by incorporating D-amino acids and N-methyls [52]. Studies are underway in our laboratory to develop highly potent and tumor-specific RID derivatives using random peptide library techniques and optimization of chemical structures.

4. Experimental protocols

4.1. Chemical synthesis

RID-F was synthesized according to the methods described in our previous reports [21,35,36]. The synthetic pathways for producing the new compounds are depicted in Schemes 1 and 2. Substituted RID-F derivatives RID-F-COOH (**15**) and RID-F-CH_2NH_2 (**19**), which could be used as precursors of peptide conjugates, were prepared using the Mukaiyama reductive coupling reaction [37,38]

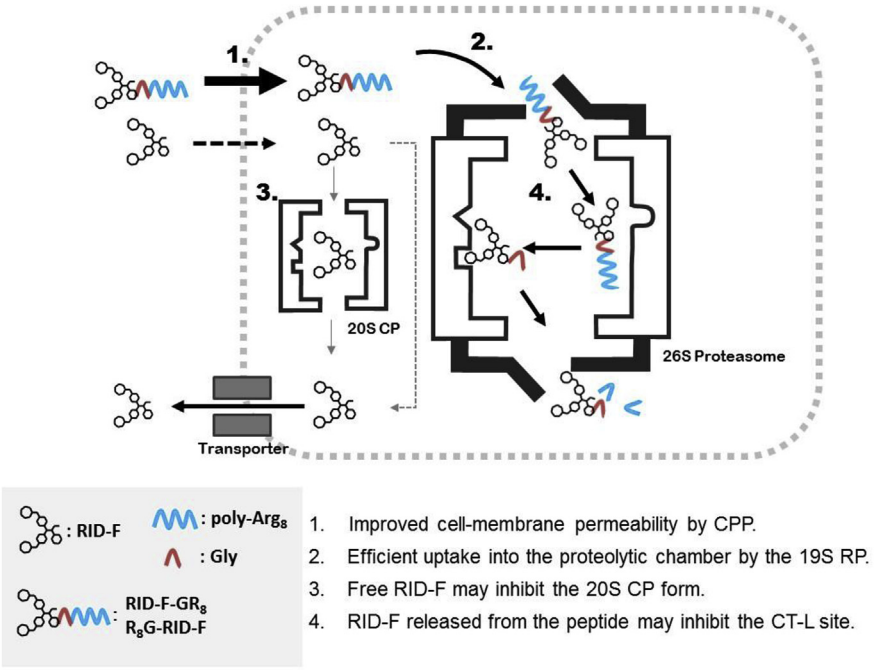

Fig. 5. Schematic illustration of the proposed mechanism via which peptide conjugates overcome multidrug resistance of KMS-11 cells. Abbreviations: CP, core particle; CPP, cell-penetrating peptide; CT-L, chymotrypsin-like activity.

and the introduction of aminoethyl ether moieties possessing azepanyl groups. The synthesis procedure of each compound is described below.

*4.1.1. (3-((4′-Methoxybenzyloxy)methyl)phenyl)methanol (**3**)*

To a solution of 1,3-phenylenedimethanol (**2**) (3.51 g, 25.4 mmol) in tetrahydrofuran (THF; 84.4 mL) at 0 °C was added 55% sodium hydride (dispersion in paraffin liquid, 1.11 g, 25.4 mmol). After dropping 4-methoxybenzyl chloride (3.43 mL, 25.4 mmol), tetrabutylammonium iodide (1.00 g, 2.71 mmol) was added. The reaction mixture was stirred for 1 h at room temperature and for 3 h at 60 °C, and then saturated aqueous ammonium chloride was added at 0 °C. The mixture was extracted with ethyl acetate, and the organic layer was dried over sodium sulfate. After filtration of the mixture and evaporation of the solvent, the crude product was purified by column chromatography on silica (eluant: hexane/ethyl acetate = 6/1) to afford **3** (2.15 g, 33%).

^{1}H NMR ($CDCl_3$, 300 MHz): δ 7.37–7.28 (6H, m, Ar), 6.92–6.88 (2H, m, Ar), 4.71 (2H, s, 1-H), 4.53 (2H, s, Bn), 4.51 (2H, s, Bn), 3.81 (3H, s, OCH_3); ^{13}C NMR ($CDCl_3$, 300 MHz): δ 159.17 (4′), 141.09, 138.58, 130.17, 129.39, 128.53, 126.95, 126.27, 126.14, 113.77 (3′), 71.85 (PMPCH_2 or PMBOCH_2), 71.66 (PMPCH_2 or PMBOCH_2), 65.04 (CH_2OH), 55.21 (CH_3O); HR MS: calcd for $C_{16}H_{18}O_3Na$ $[M+Na]^+$ 281.1148, found 281.1160.

*4.1.2. 1-(3′-((4″-Methoxybenzyloxy)methyl)phenyl)propan-1-ol (**5**)*

To a solution of dimethyl sulfoxide (DMSO; 1.16 mL, 17.7 mmol) in dichloromethane (78.0 mL) was added oxalyl chloride (1.15 mL, 13.2 mmol) at −78 °C. The reaction mixture was stirred for 20 min at −78 °C, and then a solution of **3** (2.15 g, 8.32 mmol) in dichloromethane (10.0 mL) was added. After the reaction mixture had been stirred for 15 min, triethlyamine (3.68 mL, 26.4 mmol) was added. After the reaction mixture was stirred for 3 h at room temperature, water was added at 0 °C. The mixture was extracted with dichloromethane, and the organic layer was washed with water and brine, and dried over sodium sulfate. After filtration of the mixture and evaporation of the solvent, the crude product was obtained.

To a solution of the crude product in THF (17.6 mL) was added ethylmagnesium bromide (1.0 M, 13.2 mL, 13.2 mmol) at 0 °C. After the reaction mixture had been stirred for 2 h at room temperature, saturated aqueous ammonium chloride was added at 0 °C. The mixture was extracted with ethyl acetate, and the organic layer was washed with water and brine, and dried over sodium sulfate. After filtration of the mixture and evaporation of the solvent, the crude product was purified by column chromatography on silica (eluant: hexane/ethyl acetate = 10/1) to afford **5** (2.38 g, 86%).

^{1}H NMR ($CDCl_3$, 500 MHz): δ 7.35–7.28 (6H, m, Ar), 6.91–6.88 (2H, m, Ar), 4.61 (1H, td, J = 7.0, 3.5 Hz, 1-H), 4.53 (2H, s, Bn), 4.50 (2H, s, Bn), 3.81 (3H, s, OCH_3), 1.87–1.71 (3H, m, 2-H and OH), 0.92 (3H, t, J = 7.0 Hz, 3-H); ^{13}C NMR ($CDCl_3$, 500 MHz): δ 159.20 (4″), 144.79, 138.50, 130.26, 129.42, 128.43, 126.92, 125.34, 125.21, 113.78 (3″), 75.89 (1), 71.86 (PMPCH_2 or PMBOCH_2), 71.77 (PMPCH_2 or PMBOCH_2), 55.24 (CH_3O), 31.84 (2), 10.13 (3); HR MS: calcd for $C_{18}H_{22}O_3Na$ $[M+Na]^+$ 309.1461, found 309.1457.

*4.1.3. 1-(3′-((4″-Methoxybenzyloxy)methyl)phenyl)propan-1-one (**6**)*

To a solution of DMSO (0.45 mL, 6.88 mmol) in dichloromethane (29.4 mL) was added oxalyl chloride (0.45 mL, 5.16 mmol) at −78 °C. The reaction mixture was stirred for 15 min at −78 °C, and then a solution of **5** (937 mg, 3.27 mmol) in dichloromethane (5.0 mL) was added. After the reaction mixture had been stirred for 15 min, triethlyamine (1.44 mL, 10.3 mmol) was added. After the reaction mixture was stirred for 2 h at room temperature, water was added at 0 °C. The mixture was extracted with dichloromethane, and the organic layer was washed with water and brine, and dried over sodium sulfate. After filtration of the mixture and evaporation of the solvent, the crude product was purified by column chromatography on silica (eluant: hexane/ethyl acetate = 6/1) to afford **6** (930 mg, 96%).

^{1}H NMR ($CDCl_3$, 500 MHz): δ 7.94 (1H, s, Ar), 7.90–7.88 (1H, m,

Ar), 7.57–7.55 (1H, m, Ar), 7.46–7.42 (1H, m, Ar), 7.32–7.28 (2H, m, Ar), 6.92–6.88 (2H, m, Ar), 4.57 (2H, s, Bn), 4.52 (2H, s, Bn), 3.82 (3H, s, OCH_3), 3.01 (2H, q, $J = 7.2$ Hz, 2-H), 1.23 (3H, t, $J = 7.2$ Hz, 3-H); ^{13}C NMR ($CDCl_3$, 500 MHz): δ 200.76 (1), 159.31 (4″), 138.98, 137.08, 132.15, 130.03, 129.45, 128.65, 127.22, 127.19, 113.85 (3″), 72.08 (PMPCH_2 or PMBOCH_2), 71.34 (PMPCH_2 or PMBOCH_2), 55.28 (CH_3O), 31.85 (2), 8.23 (3); HR MS: calcd for $C_{18}H_{20}O_3Na$ $[M+Na]^+$ 307.1305, found 307.1293.

4.1.4. 4,4′-(2″-(3‴-((4⁗-Methoxybenzyloxy)methyl)phenyl)but-1″-ene-1″,1″-diyl)diphenol (**8**)

To a suspension of zinc powder (2.76 g, 42.2 mmol) in THF (21.1 mL) at −10 °C was added titanium(IV) chloride (2.1 mL, 19.1 mmol). The reaction mixture was diluted with THF (5.0 mL) and refluxed at 90 °C (bath temperature) for 2 h, and then a mixture of 4,4′-dihydroxybenzophenone (**7**) (2.15 g, 10.0 mmol) and **6** (890 mg, 3.13 mmol) in THF (54.0 mL) was added to the mixture at 0 °C. After the reaction mixture had been refluxed at 90 °C (bath temperature) for 2 h in the dark, 10% aqueous potassium carbonate was added to the mixture at 0 °C in the light. The mixture was filtered through a short pad of Celite® with ethyl acetate, and the filtrate was extracted with ethyl acetate. The organic layer was washed with brine, and dried over sodium sulfate. After filtration of the mixture and evaporation of the solvent, the crude product was purified by thin-layer chromatography on silica (eluant: hexane/ethyl acetate = 6/1) to afford **8** (756 mg, 52%).

^1H NMR (CD_3OD, 500 MHz): δ 7.19–7.16 (3H, m, Ar), 7.09–7.06 (3H, m, Ar), 7.03–7.00 (2H, m, Ar), 6.88–6.86 (2H, m, Ar), 6.77–6.74 (2H, m, Ar), 6.68–6.65 (2H, m, Ar), 6.41–6.38 (2H, m, Ar), 4.36 (2H, s, Bn), 4.22 (2H, s, Bn), 3.76 (3H, s, OCH_3), 2.48 (2H, q, $J = 7.50$ Hz, 3-H), 0.90 (3H, t, $J = 7.50$ Hz, 4-H); ^{13}C NMR (CD_3OD, 300 MHz): δ 160.81 (4⁗), 157.24 (4 or 4′), 156.39 (4 or 4′), 144.51, 141.33, 140.22, 138.92, 136.47, 136.13, 133.12, 131.60, 131.38, 130.95, 130.70, 130.14, 129.03, 126.74, 115.82 (3 or 3′ or 3⁗), 115.12 (3 or 3′ or 3⁗), 114.75 (3 or 3′ or 3⁗), 72.58 (PMPCH_2 or PMBOCH_2), 72.10 (PMPCH_2 or PMBOCH_2), 55.67 (CH_3O), 29.86 (3″), 13.99 (4″); HR MS: calcd for $C_{31}H_{30}O_4Na$ $[M+Na]^+$ 489.2036, found 489.2031.

4.1.5. (((2′-(3″-((4‴-Methoxybenzyloxy)methyl)phenyl)but-1′-ene-1′,1′-diyl)bis(1,4-phenylene))bis(oxy))bis(tert-butyldimethylsilane) (**9**)

To a solution of **8** (38.1 mg, 0.0817 mmol) and imidazole (44.5 mg, 0.654 mmol) in dimethylformamide (DMF; 2.04 mL) at 0 °C were added *tert*-butylchlorodimethylsilane (49.2 mg, 0.326 mmol) and *N*,*N*-dimethyl-4-aminopyridine (DMAP; 0.20 mg, 0.00164 mmol). After the reaction mixture was stirred for 14 h at room temperature, water was added at 0 °C. The mixture was extracted with diethyl ether, and the organic layer was washed with 1 N sodium hydroxide solution, water, and brine, and dried over sodium sulfate. After filtration of the mixture and evaporation of the solvent, the crude product was purified by thin-layer chromatography on silica (eluant: hexane/ethyl acetate = 9/1) to afford **9** (46.6 mg, 82%).

^1H NMR ($CDCl_3$, 500 MHz): δ 7.24–7.21 (2H, m, Ar), 7.15–7.12 (1H, m, Ar), 7.10–7.07 (4H, m, Ar), 7.03–7.01 (1H, m, Ar), 6.88–6.87 (2H, m, Ar), 6.82–6.79 (2H, m, Ar), 6.72–6.69 (2H, m, Ar), 6.47–6.44 (2H, m, Ar), 4.40 (2H, s, Bn), 4.31 (2H, s, Bn), 3.81 (3H, s, OCH_3), 2.48 (2H, q, $J = 7.5$ Hz, 3-H), 1.00 (9H, s, TBS), 0.92 (3H, t, $J = 7.5$ Hz, 4-H), 0.89 (9H, s, TBS), 0.22 (6H, s, TBS), 0.06 (6H, s, TBS); ^{13}C NMR ($CDCl_3$, 500 MHz): δ 159.15 (4‴), 154.26 (1), 153.48 (1), 142.80, 140.78, 138.23, 137.69, 136.71, 136.37, 131.89, 130.53, 130.42, 129.44, 129.23, 129.02, 127.84, 125.44, 119.46 (2), 118.85 (2), 113.75 (3‴), 71.66 (PMPCH_2 or PMBOCH_2), 71.13 (PMPCH_2 or PMBOCH_2), 55.27 (CH_3O), 28.91 (3′), 25.68 and 25.63 (Si(CH_3)$_2$C(CH_3)$_3$), 18.18 and 18.12 (Si(CH$_3$)$_2$*C*(CH$_3$)$_3$), 13.65 (4′), −4.38 and −4.52 (Si(CH_3)$_2$C(CH_3)$_3$); HR MS: calcd for $C_{43}H_{58}O_4Si_2Na$ $[M+Na]^+$ 717.3766, found 717.3735.

4.1.6. (3-(1′,1′-Bis(4″-(tert-butyldimethylsilyloxy)phenyl)but-1′-en-2′-yl)phenyl)methanol (**10**)

To a solution of **9** (182 mg, 0.262 mmol) in dichloromethane/phosphate buffer (pH 7; 9/1 ratio; 6.55 mL) was added 2,3-dichloro-5,6-dicyano-1,4-benzoquinone (DDQ; 119 mg, 0.524 mmol) at 0 °C. After the reaction mixture was stirred for 1.5 h at room temperature, phosphate buffer (pH 7) was added at 0 °C. The mixture was extracted with dichloromethane, and the organic layer was washed with brine and dried over sodium sulfate. After filtration of the mixture and evaporation of the solvent, the crude product was purified by thin-layer chromatography on silica (eluant: hexane/ethyl acetate = 3/1) to afford **10** (109 mg, 72%).

^1H NMR ($CDCl_3$, 400 MHz): δ 7.16–7.00 (6H, m, Ar), 6.82–6.80 (2H, m, Ar), 6.71–6.67 (2H, m, Ar), 6.48–6.45 (2H, m, Ar), 4.53 (2H, d, $J = 5.6$ Hz, CH_2O), 2.49 (2H, q, $J = 7.3$ Hz, 3-H), 0.99 (9H, s, TBS), 0.94–0.91 (12H, 4-H and TBS), 0.22 (6H, s, TBS), 0.09 (6H, s, TBS); ^{13}C NMR ($CDCl_3$, 400 MHz): δ 154.27 and 153.51 (4″), 142.99, 140.64, 140.26, 138.41, 136.61, 136.42, 131.87, 130.49, 129.02, 128.49, 127.97, 124.53, 119.47 and 118.89 (3″), 65.40 (*C*H_2OH), 28.73 (3′), 25.66 and 25.64 (Si(CH_3)$_2$C(*C*H$_3$)$_3$), 18.17 and 18.15 (Si(CH$_3$)$_2$*C*(CH$_3$)$_3$), 13.67 (4′), −4.39 and −4.51 (Si(*C*H$_3$)$_2$C(CH$_3$)$_3$); HR MS: calcd for $C_{35}H_{50}O_3Si_2Na$ $[M+Na]^+$ 597.3191, found 597.3184.

4.1.7. 3-(1′,1′-Bis(4″-(tert-butyldimethylsilyloxy)phenyl)but-1′-en-2′-yl)benzaldehyde (**11**)

To a solution of **10** (99.4 mg, 0.173 mmol) in dichloromethane (3.46 mL) was added Dess–Martin periodinane (DMP; 117 mg, 0.277 mmol) at room temperature. After the reaction mixture was stirred for 2 h at room temperature, diethyl ether and 10% sodium thiosulfate/saturated aqueous sodium hydrogen carbonate at a 1/1 ratio (volume) were added at 0 °C. The mixture was extracted with diethyl ether, and the organic layer was washed twice with brine, and dried over sodium sulfate. After filtration of the mixture and evaporation of the solvent, the crude product was purified by thin-layer chromatography on silica (eluant: hexane/ethyl acetate = 10/1) to afford **11** (93.1 mg, 94%).

^1H NMR ($CDCl_3$, 500 MHz): δ 9.87 (1H, s, CHO), 7.62–7.60 (2H, m, Ar), 7.35–7.29 (2H, m, Ar), 7.11–7.08 (2H, m, Ar), 6.83–6.80 (2H, m, Ar), 6.71–6.68 (2H, m, Ar), 6.49–6.46 (2H, m, Ar), 2.54 (2H, q, $J = 7.5$ Hz, 3-H), 1.00 (9H, s, TBS), 0.93 (3H, t, $J = 7.5$ Hz, 4-H), 0.90 (9H, s, TBS), 0.23 (6H, s, TBS), 0.08 (6H, s, TBS); ^{13}C NMR ($CDCl_3$, 500 MHz): δ 192.44 (*C*HO), 154.53 and 153.86 (4″), 143.90, 139.69, 139.44, 136.16, 136.13, 136.10, 135.80, 131.95, 131.15, 130.43, 128.56, 127.14, 119.55 and 119.16 (3″), 28.59 (3′), 25.66 and 25.64 (Si(CH_3)$_2$C(*C*H$_3$)$_3$), 18.18 (Si(CH$_3$)$_2$*C*(CH$_3$)$_3$), 13.57 (4′), −4.38 and −4.50 (Si(*C*H$_3$)$_2$C(CH$_3$)$_3$); HR MS: calcd for $C_{35}H_{48}O_3Si_2Na$ $[M+Na]^+$ 595.3034, found 595.3039.

4.1.8. Benzyl 3-(1′,1′-bis(4″-(tert-butyldimethylsilyloxy)phenyl)but-1′-en-2′-yl)benzoate (**13**)

To a solution of **11** (16.0 mg, 0.0279 mmol) in THF (0.47 mL) were added 2-methyl-2-butene (0.030 mL, 0.279 mmol), *tert*-butyl alcohol (0.47 mL), sodium chlorite (6.3 mg, 0.0559 mmol), and a solution of sodium dihydrogen phosphate (16.6 mg, 0.140 mmol) in water (0.47 mL). After the reaction mixture had been stirred for 3.5 h, brine was added at 0 °C. The mixture was extracted with chloroform, and the organic layer was dried over sodium sulfate. After filtration of the mixture and evaporation of the solvent, the crude product was obtained.

To a solution of the crude product in DMF (1.00 mL) were added 55% sodium hydride (dispersion in paraffin liquid, 2.9 mg, 0.0670 mmol) and benzyl bromide (3.98 μL, 0.0335 mmol). After the reaction mixture had been stirred for 11 h, saturated aqueous

ammonium chloride was added at 0 °C. The mixture was extracted with ethyl acetate, and the organic layer was dried over sodium sulfate. After filtration of the mixture and evaporation of the solvent, the crude product was purified by thin-layer chromatography on silica (eluant: hexane/ethyl acetate = 4/1) to afford **13** (15.2 mg, 80%).

^{1}H NMR ($CDCl_3$, 500 MHz): δ 7.87–7.87 (1H, m, Ar), 7.81–7.79 (1H, m, Ar), 7.44–7.33 (6H, m, Ar), 7.24–7.22 (1H, m, Ar), 7.18–7.15 (1H, m, Ar), 7.09–7.08 (2H, m, Ar), 6.82–6.80 (2H, m, Ar), 6.70–6.67 (2H, m, Ar), 6.48–6.46 (2H, m, Ar), 5.32 (2H, s, Bn), 2.52 (2H, q, J = 7.5 Hz, 3-H), 1.00 (9H, s, TBS), 0.93–0.90 (12H, m, 4-H and TBS), 0.22 (6H, s, TBS), 0.07 (6H, s, TBS); ^{13}C NMR ($CDCl_3$, 500 MHz): δ 166.53 (*C*OOBn), 154.40 and 153.68 (4″), 143.14, 139.85, 139.22, 136.28, 136.10, 135.99, 134.85, 131.94, 130.69, 130.45, 129.65, 128.56, 128.14, 128.08, 127.81, 127.24, 119.48 and 119.08 (3″), 66.54 (Ph*C*H$_2$O), 28.64 (3′), 25.66 and 25.63 (Si(CH$_3$)$_2$C(*C*H$_3$)$_3$), 18.17 and 18.15 (Si(CH$_3$)$_2$*C*(CH$_3$)$_3$), 13.59 (4′), −4.38 and −4.52 (Si(*C*H$_3$)$_2$C(CH$_3$)$_3$); HR MS: calcd for $C_{42}H_{54}O_4Si_2Na$ [M+Na]$^+$ 703.3482, found 703.3588.

4.1.9. Benzyl 3-(1′,1′-bis(4″-hydroxyphenyl)but-1′-en-2′-yl) benzoate (**14**)

To a solution of **13** (52.1 mg, 0.0767 mmol) in THF (2.50 mL) at room temperature was added tetrabutylammonium fluoride (TBAF) in THF (1.0 M, 0.30 mL, 0.300 mmol) at 0 °C. The reaction mixture was stirred for 1 h at room temperature, and saturated aqueous ammonium chloride was added at 0 °C. The mixture was extracted with ethyl acetate, and the organic layer was dried over sodium sulfate. After filtration of the mixture and evaporation of the solvent, the crude product was purified by thin-layer chromatography on silica (eluant: hexane/ethyl acetate = 1/2) to afford **14** (21.0 mg, 61%).

^{1}H NMR ($CDCl_3$, 500 MHz): δ 7.88–7.87 (1H, m, Ar), 7.82–7.80 (1H, m, Ar), 7.43–7.33 (5H, m, Ar), 7.26–7.24 (1H, m, Ar), 7.21–7.18 (1H, m, Ar), 7.10–7.08 (2H, m, Ar), 6.81–6.79 (2H, m, Ar), 6.70–6.68 (2H, m, Ar), 6.46–6.43 (2H, m, Ar), 5.32 (2H, s, Bn), 2.51 (2H, q, J = 7.5 Hz, 3-H), 0.90 (3H, t, J = 7.5 Hz, 4-H); ^{13}C NMR (CD_3OD, 500 MHz): δ 167.85 (*C*OOBn), 157.41 and 156.61 (4″), 144.86, 141.26, 140.26, 137.60, 136.08, 135.83, 135.65, 133.17, 132.24, 131.56, 130.89, 129.62, 129.18, 128.98, 128.09, 115.83 and 115.27 (3″), 67.61 (Ph*C*H$_2$O), 29.56 (3′), 13.98 (4′); HR MS: calcd for $C_{30}H_{26}O_4Na$ [M+Na]$^+$ 473.1723, found 473.1744.

4.1.10. 3-(1′,1′-Bis(4″-(2‴-(azepan-1⁗-yl)ethoxy)phenyl)but-1′-en-2′-yl)benzoic acid (RID-F-COOH, **15**)

To a solution of **14** (21.0 mg, 0.0466 mmol) in DMF (1.20 mL) was added 55% sodium hydride (dispersion in paraffin liquid, 12.2 mg, 0.280 mmol). The reaction mixture was stirred for 15 min at 50 °C, and then 1-(2-chloroethyl)azepane hydrochloride (30.5 mg, 0.154 mmol) was added in portions at room temperature. After the reaction mixture had been stirred for 3 h at 50 °C, saturated aqueous ammonium chloride was added at 0 °C. The mixture was extracted with dichloromethane, and the organic layer was dried over sodium sulfate. After filtration of the mixture and evaporation of the solvent, the crude product was purified by thin-layer chromatography on silica (eluant: ammoniacal chloroform/methanol = 9/1) to afford the crude product (96.4 mg). After removing the solid (57.6 mg) precipitated from the mixture, the residue was azeotroped with toluene to afford RID-F-COOH (**15**) (22.1 mg, 77%).

^{1}H NMR ($CDCl_3$, 500 MHz): δ 11.59 (1H, br s, COOH), 7.90 (1H, s, Ar), 7.79 (1H, d, J = 7.5 Hz, Ar), 7.17–7.10 (3H, m, Ar), 7.06–7.04 (1H, m, Ar), 6.86–6.83 (2H, m, Ar), 6.76–6.74 (2H, m, Ar), 6.48–6.46 (2H, m, Ar), 4.31 (2H, t, J = 4.5 Hz, OCH$_2$), 4.16 (2H, t, J = 4.5 Hz, OCH$_2$), 3.37–3.33 (4H, m, NCH$_2$), 3.23–3.21 (8H, m, azepanyl), 2.48 (2H, q, J = 7.2 Hz, 3-H), 1.88–1.83 (8H, m, azepanyl), 1.69–1.65 (8H, m, azepanyl), 0.89 (3H, t, J = 7.2 Hz, 4-H); ^{13}C NMR ($CDCl_3$, 500 MHz): δ 156.51 and 155.57 (4″), 141.99, 141.35, 137.48, 136.83, 136.30, 133.18, 132.10, 130.64, 130.04, 128.99, 128.18, 127.54, 125.26, 114.05 and 113.38 (3″), 63.91 and 63.61 (1‴), 55.35 and 55.13 (2‴), 54.70 and 54.46 (azepane), 29.66 (3′), 27.06 and 27.02 (azepane), 24.14 and 23.62 (azepane), 13.58 (4′); HR MS: calcd for $C_{39}H_{51}N_2O_4$ [M+H]$^+$ 611.3843, found 611.3856.

4.1.11. (E)-3-(1′,1′-Bis(4″-(tert-butyldimethylsilyloxy)phenyl)but-1′-en-2′-yl)benzaldehyde O-benzyl oxime (**16a**) and (E)-3-((E)-1′-(4″-(tert-Butyldimethylsilyloxy)phenyl)-1′-(4‴-hydroxyphenyl)but-1′-en-2′-yl)benzaldehyde O-benzyl oxime or (E)-3-((Z)-1′-(4″-(tert-Butyldimethylsilyloxy)phenyl)-1′-(4‴-hydroxyphenyl)but-1′-en-2′-yl)benzaldehyde O-benzyl oxime (**16b**)

To a solution of **11** (43.3 mg, 0.0756 mmol) in methanol (0.76 mL) at room temperature were added *O*-benzylhydroxylamine (18.6 mg, 0.151 mmol) and sodium carbonate (32.0 mg, 0.302 mmol). The reaction mixture was stirred for 19 h at room temperature, and then brine was added at 0 °C. The mixture was extracted with ethyl acetate, and the organic layer was dried over sodium sulfate. After filtration of the mixture and evaporation of the solvent, the crude product was purified by thin-layer chromatography on silica (eluant: hexane/ethyl acetate = 10/1) to afford **16a** (17.6 mg, 34%) and **16b** (22.2 mg, 52%).

4.1.12. **16a**

^{1}H NMR ($CDCl_3$, 400 MHz): δ 8.01 (1H, s, 5-H), 7.44–7.31 (7H, m, Ar), 7.14–7.04 (4H, m, Ar), 6.83–6.80 (2H, m, Ar), 6.72–6.69 (2H, m, Ar), 6.50–6.47 (2H, m, Ar), 5.19 (2H, s, Bn), 2.51 (2H, q, J = 7.6 Hz, 3-H), 1.01 (9H, s, TBS), 0.95–0.92 (12H, m, TBS and 4-H), 0.23 (6H, s, TBS), 0.10 (6H, s, TBS); ^{13}C NMR (CD_3OD, 400 MHz): δ 154.35 and 153.66 (4″), 149.25 (*C*HNOBn), 143.25, 140.14, 138.78, 137.52, 136.45, 136.10, 131.86, 131.69, 131.64, 130.48, 128.54, 128.40, 128.10, 127.92, 124.39, 119.48 and 119.02 (3″), 76.31 (Ph*C*H$_2$O), 28.72 (3′), 25.67 (Si(CH$_3$)$_2$C(*C*H$_3$)$_3$), 18.17 (Si(CH$_3$)$_2$*C*(CH$_3$)$_3$), 13.61 (4′), −4.38 and −4.48 (Si(*C*H$_3$)$_2$C(CH$_3$)$_3$); HR MS: calcd for $C_{42}H_{56}NO_3Si_2$ [M+H]$^+$ 678.3793, found 678.3815.

4.1.13. **16b**

^{1}H NMR ($CDCl_3$, 400 MHz): δ 8.02 (1H, s, 5-H *E* or *Z*), 8.00 (1H, s, 5-H *E* or *Z*), 7.43–7.28 (8H, m, Ar), 7.13–7.05 (4H, m, Ar), 6.82–6.79 (2H, m, Ar), 6.73–6.68 (2H, m, Ar), 6.48–6.45 (2H, m, Ar), 5.19 (2H, s, Bn *E* or *Z*), 5.18 (2H, s, Bn *E* or *Z*), 4.70 (1H, s, OH *E* or *Z*), 4.47 (1H, s, OH *E* or *Z*), 2.48 (2H, q, J = 7.6 Hz, 3-H), 0.99–0.90 (12H, m, TBS and 4-H *E* or *Z*), 0.22 and 0.08 (6H, s, TBS *E* or *Z*); ^{13}C NMR ($CDCl_3$, 500 MHz): δ 154.34 and 154.25 and 153.63 and 153.46 (4″ or 4‴), 149.31 (*C*HNOBn), 143.18, 143.11, 140.23, 140.16, 138.48, 137.41, 136.43, 136.04, 135.59, 132.12, 131.84, 131.66, 130.71, 130.45, 128.42, 128.30, 128.19, 128.13, 127.94, 127.88, 124.47, 119.52 and 119.06 (3″), 114.90 and 114.29 (3‴), 76.29 (Ph*C*H$_2$O), 28.82 and 28.71 (3′), 25.65 (Si(CH$_3$)$_2$C(*C*H$_3$)$_3$), 18.17 (Si(CH$_3$)$_2$*C*(CH$_3$)$_3$), 13.61 (4′), −4.39 and −4.49 (Si(*C*H$_3$)$_2$C(CH$_3$)$_3$); HR MS: calcd for $C_{36}H_{41}NO_3SiNa$ [M+Na]$^+$ 586.2748, found 586.2762.

4.1.14. (E)-3-(1′,1′-Bis(4″-hydroxyphenyl)but-1′-en-2′-yl) benzaldehyde O-benzyl oxime (**17**)

To a solution of **16a** (16.3 mg, 0.0240 mmol) in THF (0.60 mL) at room temperature was added TBAF in THF (1.0 M, 72.1 μL, 0.0721 mmol) at 0 °C. The reaction mixture was stirred for 30 min at room temperature, and saturated aqueous ammonium chloride was added at 0 °C. The mixture was extracted with dichloromethane, and the organic layer was dried over sodium sulfate. After filtration of the mixture and evaporation of the solvent, the crude product was purified by thin-layer chromatography on silica (eluant: hexane/ethyl acetate = 2/1) to afford **17** (9.5 mg, 88%).

To a solution of **16b** (22.2 mg, 0.0394 mmol) in THF (0.98 mL) at room temperature was added TBAF in THF (1.0 M, 59.1 μL, 0.0591 mmol) at 0 °C. The reaction mixture was stirred for 30 min at room temperature, and saturated aqueous ammonium chloride was added at 0 °C. The mixture was extracted with dichloromethane, and the organic layer was dried over sodium sulfate. After filtration of the mixture and evaporation of the solvent, the crude product was purified by thin-layer chromatography on silica (eluant: hexane/ethyl acetate = 2/1) to afford **17** (15.2 mg, 86%).

^{1}H NMR ($CDCl_3$, 400 MHz): δ 8.03 (1H, s, 5-H), 7.43–7.30 (7H, m, Ar), 7.15–7.05 (4H, m, Ar), 6.82–6.78 (2H, m, Ar), 6.73–6.70 (2H, m, Ar), 6.47–6.44 (2H, m, Ar), 5.19 (2H, s, Bn), 2.48 (2H, q, J = 7.6 Hz, 3-H), 0.92 (3H, t, J = 7.6 Hz, 4-H); ^{13}C NMR ($CDCl_3$, 400 MHz): δ 154.35 and 153.55 (4″), 149.36 (*C*HNOBn), 143.15, 140.32, 138.33, 137.47, 136.09, 135.58, 132.10, 131.72, 131.68, 130.71, 128.43, 128.38, 128.22, 127.95, 124.61, 114.99 and 114.37 (3″), 76.33 (Ph*C*H_2O), 28.83 (3′), 13.58 (4′); HR MS: calcd for $C_{30}H_{27}NO_3Na$ $[M+Na]^+$ 472.1883, found 472.1890.

4.1.15. (E)-3-(1′,1′-Bis(4″-(2‴-(azepan-1⁗-yl)ethoxy)phenyl)but-1′-en-2′-yl)benzaldehyde O-benzyl oxime (**18**)

To a solution of **17** (8.5 mg, 0.0189 mmol) in DMF (0.4 mL) was added 55% sodium hydride (dispersion in paraffin liquid, 8.3 mg, 0.189 mmol). The reaction mixture was stirred for 15 min at 50 °C, and then 1-(2-chloroethyl)azepane hydrochloride (18.7 mg, 0.0945 mmol) was added in portions at room temperature. After the reaction mixture had been stirred for 12 h at 50 °C, saturated aqueous ammonium chloride was added at 0 °C. The mixture was extracted with dichloromethane, and the organic layer was dried over sodium sulfate. After filtration of the mixture and evaporation of the solvent, the crude product was purified by thin-layer chromatography on silica (eluant: ammoniacal chloroform/methanol = 30/1) to afford **18** (10.2 mg, 77%).

^{1}H NMR ($CDCl_3$, 400 MHz): δ 7.42–7.24 (9H, m, Ar), 7.12–6.87 (2H, m, Ar), 6.73–6.70 (2H, m, Ar), 6.57–6.55 (2H, m, Ar), 4.54 (2H, s, Bn), 4.08 (2H, t, J = 6.4 Hz, OCH_2), 3.94 (2H, t, J = 6.4 Hz, OCH_2), 2.97 (2H, t, J = 6.4 Hz, NCH_2), 2.88 (2H, t, J = 6.4 Hz, NCH_2), 2.80–2.69 (8H, m, azepanyl 2-H), 2.49 (2H, q, J = 7.6 Hz, 3-H), 1.67–1.59 (16H, m, azepanyl 3-H and 4-H), 0.92 (3H, t, J = 7.6 Hz, 4-H); ^{13}C NMR ($CDCl_3$, 400 MHz): δ 157.94 and 157.27 (4″), 144.26 (*C*HNOBn), 140.12, 138.51, 138.48, 135.35, 134.69, 134.48, 133.11, 131.91, 131.74, 130.47, 130.38, 129.56, 128.67, 128.42, 128.33, 127.94, 127.65, 127.51, 119.06, 114.16 and 113.69 (3″), 73.13 (Ph*C*H_2O), 66.44 and 66.21 (1‴), 56.42 and 56.27 (2‴), 55.88 and 55.83 (azepane), 29.68 (3′), 27.95 and 27.88 (azepane), 27.03 (azepane), 13.51 (4′); HR MS: calcd for $C_{46}H_{58}N_3O_3$ $[M+H]^+$ 700.4473, found 700.4497.

4.1.16. (3-(1′,1′-Bis(4″-(2‴-(azepan-1⁗-yl)ethoxy)phenyl)but-1′-en-2′-yl)phenyl)methanamine (RID-F-CH_2NH_2, **19**)

To a solution of **18** (9.7 mg, 0.0139 mmol) in THF (0.34 mL) at 0 °C was added lithium aluminum hydride (1.6 mg, 0.0422 mmol). The reaction mixture was stirred for 3 h at room temperature, and saturated aqueous potassium sodium tartrate was added at 0 °C. The mixture was extracted with dichloromethane, and the organic layer was dried over sodium sulfate. After filtration of the mixture and evaporation of the solvent, the crude product was purified by thin-layer chromatography on silica (eluant: ammoniacal chloroform/methanol = 30/1) to afford RID-F-CH_2NH_2 (**19**) (6.4 mg, 77%).

^{1}H NMR ($CDCl_3$, 400 MHz): δ 7.16–7.12 (3H, m, Ar), 7.02–7.00 (3H, m, Ar), 6.90–6.86 (2H, m, Ar), 6.77–6.73 (2H, m, Ar), 6.55–6.52 (2H, m, Ar), 4.09 (2H, t, J = 6.0 Hz, OCH_2), 3.93 (2H, t, J = 6.0 Hz, OCH_2), 3.70 (2H, s, 5-H), 2.98 (2H, t, J = 6.0 Hz, NCH_2), 2.87 (2H, t, J = 6.0 Hz, NCH_2), 2.80 (4H, q, azepanyl 2-H), 2.73 (4H, q, azepanyl 2-H), 2.49 (2H, q, J = 7.6 Hz, 3-H), 1.68–1.56 (16H, m, azepanyl 3-H and 4-H), 0.93 (3H, t, J = 7.6 Hz, 4-H); ^{13}C NMR ($CDCl_3$, 500 MHz): δ 157.57 and 156.76 (4″), 142.79, 140.84, 137.98, 136.17, 135.88, 131.84, 130.52, 130.46, 128.73, 127.93, 124.59, 114.03 and 113.32 (3″), 66.36 and 66.18 (1‴), 56.45 and 56.31 (2‴), 55.87 and 55.81 (azepane), 46.48 (*C*H_2NH_2), 28.78 (3′), 27.94 and 27.88 (azepane), 27.05 (azepane), 13.71 (4′); HR MS: calcd for $C_{39}H_{54}N_3O_2$ $[M+H]^+$ 596.4211, found 596.4207.

4.2. Synthesis of RID-F-peptide conjugates

To obtain peptide conjugates, peptides were reacted with an equimolar RID-F derivative carrying a carboxy group or amino group, 1-(3′-dimethylaminopropyl)-3-ethylcarbodiimide and 1-hydroxybenzotriazole in DMF containing 100 equivalents of triethylamine. All peptides were synthesized using 9-fluorenylmethoxycarbonyl (Fmoc) chemistry according to standard methods. After incubating for 6 h at 40 °C, the target conjugates were purified from reaction mixtures with a HPLC system (Gilson, Inc., WI, USA) equipped with a reverse phase column (COSMOSIL, $_5C_{18}$-AR-II, 4.6 × 150 mm, Nacalai Tesque Inc., Kyoto, Japan). HPLC was performed at a flow rate of 1 mL/min with a linear gradient of 5–50% acetonitrile in 0.05% trifluoroacetic acid in water. Purities of the target conjugates were confirmed using a Spiral-TOF JMS-S3000 mass spectrometer (JEOL Ltd., Tokyo, Japan).

4.3. Cell culture

RPMI8226 and KMS-11 cell lines were distributed by RIKEN BRC Cell Bank (Chiba, Japan) and JCRB Cell Bank, National Institutes of Biomedical Innovation, Health and Nutrition (Osaka, Japan), respectively. Cells were grown and maintained in RPMI1640 medium (Nacalai Tesque, Kyoto, Japan) supplemented with 10% fetal bovine serum, 100 units/mL penicillin, and 100 μg/mL streptomycin at 37 °C in 5% CO_2.

4.4. Proteasome fluorometric substrate assays

The CT-L, PGPH, and T-L proteasome activities were determined by measuring the degradation rate of the fluorometric substrates, Suc-LLVY-MCA, Z-LLE-MCA, and Boc-LRR-MCA, respectively. Purified human 20S proteasomes (0.1 μg; Enzo Life Sciences, Inc., NY, USA) were incubated with a fluorometric peptide substrate (50 μM) in the presence of varying concentrations of inhibitory compounds (0.1–10 μM) in 100 μL of assay buffer (25 mM HEPES [pH 8.0], 0.5 mM ethylenediaminetetraacetic acid, 0.03% SDS) [40]. The reaction mixture was monitored for the fluorescence of released 7-amino-4-methylcoumarin (λ_{ex} = 380 nm, λ_{em} = 480 nm) for 1 h at 37 °C. Inhibitory potencies of the compounds (0.1–40 μM) for purified 26S proteasomes (0.1 μg) were measured using similar conditions to those described above but with another assay buffer (50 mM HEPES [pH 7.5], 40 mM KCl, 5 mM $MgCl_2$, 50 μg of bovine serum albumin, 0.5 mM ATP, 1 mM dithiothreitol) with the corresponding fluorometric peptide substrate (50 μM). The IC_{50} value, defined as the compound concentration required for 50% inhibition of proteasome activity, was determined for each compound from the respective inhibition curve.

4.5. Cell growth inhibition assays

RPMI8226 and KMS-11 cells were seeded in triplicate wells in a 96-well plate at a density of 5 × 10^2 cells/well and incubated with various concentrations (0.1–10 μM) of inhibitory compounds dissolved in DMSO for 24 or 48 h. The amounts of intracellular ATP were determined by CellTiter-Glo® Luminescent Cell Viability Assay (Promega Co., WI, USA) according to the manufacturer's protocol.

4.6. Measurements of intracellular proteasome activity

RPMI8226 and KMS-11 [53] cells were seeded in triplicate wells in a 96-well plate at a density of 5×10^3 cells/well and incubated for 24 or 48 h in the corresponding medium with various concentrations (0.1–10 μM) of inhibitors dissolved in DMSO. The final concentration of DMSO was 0.5% in each reaction mixture. The Proteasome-Glo™ Assay (Promega Co.) reagent [42] was mixed according to the manufacturer's protocol. In this assay, cell lysis is achieved directly at the step of addition of substrates, which consists of peptides bound to aminoluciferin, with a detergent-containing buffer. Aminoluciferin dye production, which is the substrate of the buffer-contained luciferase, was measured after incubation for 15 min.

4.7. Molecular docking simulations

To dock RID-F-GR and RG-RID-F with the CT-L site of the human 20S proteasome, using AutoDock Vina version 1.1.2 (ADV) [43], structural data were prepared as follows.

From the known human 20S proteasome structure data, the complexed structure with dihydroeponemycin (PDB ID: 5lf1 [44]) determined at 2.0 Å resolution was selected. As the cleft formed by the β5 and β6 subunits (chain K and L, respectively) was used for binding to dihydroeponemycin, the cleft was considered as the CT-L site, and the dimer structure of chains K and L was used for docking. The dimer structure was rotated to fit the binding site of dihydroeponemycin into the docking grid box ($24 \times 24 \times 20$ Å) for the ADV run (Fig. 4) and converted to PDBQT format using MGL Tools version 1.5.6 [54]. The center coordinates of the docking grid box were determined on the basis of the center of the amino acid residues bound to dihydroeponemycin. To prevent a part of the ligand from binding to the outside of the proteasome chamber, the center coordinates of the docking grid box were slightly moved manually.

To handle the dipeptide moiety (Gly-Arg) of RID-F-GR in the ADV calculation properly, 3D atomic coordinates of RID-F-GR were generated using two steps. First, 3D atomic coordinates of RID-F-G were generated from the two-dimensional representation using Balloon [55] with default parameters. Second, 3D atomic coordinates of Arg were added to the C-terminal of Gly in the RID-F-G structure using the Protein Builder function in Molecular Operating Environment software, version 2015.1001 (MOE 2015.1001). Moreover, the Conformational Search function with the Low-ModeMD of MOE 2015.1001 was performed to obtain an initial structure of the docking. The first ranked structure obtained from the Conformational Search was converted to PDBQT format using MGL Tools. In the same way, 3D atomic coordinates of RG-RID-F for the initial structure of the docking were generated using Balloon and MOE 2015.1001.

Ten ADV runs were calculated with default parameters except for exhaustiveness (1024) and num_modes (10). One hundred docking poses obtained from 10 ADV runs were clustered by complete linkage clustering using Root Mean Square Deviation lower bound (l.b. RMSD) values between each docking pose and grouped with cut-off values of 2.0 l.b. RMSD. The highest-score docking pose from the largest cluster was selected as an estimated binding mode.

Conflicts of interest

The authors declare no competing financial interests.

Acknowledgments

The authors thank Shigehito Sugiyama, Mie Tsuchida, and Miho Hosoi for technical assistance. This study was supported by a Grant-in-Aid for Scientific Research (C), JSPS KAKENHI (JP16K08329) to M.H., and a Health and Labour Sciences Research Grant from the Ministry of Health, Labour, and Welfare, Japan (11103425) to I.S. M.S. received support from the Platform Project for Supporting Drug Discovery and Life Science Research (Basis for Supporting Innovative Drug Discovery and Life Science Research [BINDS]) from the Japan Agency for Medical Research and Development (AMED).

Abbreviations

ATP, adenosine triphosphate; ATPγS, adenosine 5′-*O*-(3-thio) triphosphate, CPP, cell-penetrating peptide; CT-L, chymotrypsin-like; Cyt_{50}, half-maximum cytotoxic concentration; DMF, dimethylformamide; DMSO, dimethyl sulfoxide, HPLC, high-performance liquid chromatography; IC_{50}, half-maximum inhibitory concentration; PGPH, peptidylglutamyl peptide hydrolase; PI, proteasome inhibitor; R_8, octaarginine; RP, regulatory particle; RID, ridaifen; SDS, sodium dodecyl sulfate; T-L, trypsin-like; THF, tetrahydrofuran.

Appendix A. Supplementary data

Supplementary data related to this article can be found at https://doi.org/10.1016/j.ejmech.2018.01.045.

References

[1] A. Hershko, A. Ciechanover, The ubiquitin system, Annu. Rev. Biochem. 67 (1998) 425–479. https://doi.org/10.1146/annurev.biochem.67.1.425.
[2] J.M. Peters, Z. Cejka, J.R. Harris, J.A. Kleinschmidt, W. Baumeister, Structural features of the 26 S proteasome complex, J. Mol. Biol. 234 (1993) 932–937. https://doi.org/10.1006/jmbi.1993.1646.
[3] D. Voges, P. Zwickl, W. Baumeister, The 26S proteasome: a molecular machine designed for controlled proteolysis, Annu. Rev. Biochem. 68 (1999) 1015–1068. https://doi.org/10.1146/annurev.biochem.68.1.1015.
[4] D. Finley, Recognition and processing of ubiquitin-protein conjugates by the proteasome, Annu. Rev. Biochem. 78 (2009) 477–513. https://doi.org/10.1146/annurev.biochem.78.081507.101607.
[5] M. Orlowski, The multicatalytic proteinase complex, a major extralysosomal proteolytic system, Biochemistry 29 (1990) 10289–10297.
[6] M. Groll, L. Ditzel, J. Lowe, D. Stock, M. Bochtler, H.D. Bartunik, R. Huber, Structure of 20S proteasome from yeast at 2.4 A resolution, Nature 386 (1997) 463–471. https://doi.org/10.1038/386463a0.
[7] R. Verma, L. Aravind, R. Oania, W.H. McDonald, J.R. Yates 3rd, E.V. Koonin, R.J. Deshaies, Role of Rpn11 metalloprotease in deubiquitination and degradation by the 26S proteasome, Science 298 (2002) 611–615. https://doi.org/10.1126/science.1075898.
[8] T. Yao, R.E. Cohen, A cryptic protease couples deubiquitination and degradation by the proteasome, Nature 419 (2002) 403–407. https://doi.org/10.1038/nature01071.
[9] G.C. Lander, E. Estrin, M.E. Matyskiela, C. Bashore, E. Nogales, A. Martin, Complete subunit architecture of the proteasome regulatory particle, Nature 482 (2012) 186–191. https://doi.org/10.1038/nature10774.
[10] K. Lasker, F. Forster, S. Bohn, T. Walzthoeni, E. Villa, P. Unverdorben, F. Beck, R. Aebersold, A. Sali, W. Baumeister, Molecular architecture of the 26S proteasome holocomplex determined by an integrative approach, Proc. Natl. Acad. Sci. U. S. A. 109 (2012) 1380–1387. https://doi.org/10.1073/pnas.1120559109.
[11] A.F. Kisselev, W.A. van der Linden, H.S. Overkleeft, Proteasome inhibitors: an expanding army attacking a unique target, Chem. Biol 19 (2012) 99–115. https://doi.org/10.1016/j.chembiol.2012.01.003.
[12] T. Hideshima, D. Chauhan, P. Richardson, C. Mitsiades, N. Mitsiades, T. Hayashi, N. Munshi, L. Dang, A. Castro, V. Palombella, J. Adams, K.C. Anderson, NF-kappa B as a therapeutic target in multiple myeloma, J. Biol. Chem. 277 (2002) 16639–16647. https://doi.org/10.1074/jbc.M200360200.
[13] A.L. Goldberg, Development of proteasome inhibitors as research tools and cancer drugs, J. Cell Biol. 199 (2012) 583–588. https://doi.org/10.1083/jcb.201210077.
[14] A. Navon, A. Ciechanover, The 26 S proteasome: from basic mechanisms to drug targeting, J. Biol. Chem. 284 (2009) 33713–33718. https://doi.org/10.1074/jbc.R109.018481.
[15] J. Adams, P.J. Elliott, New agents in cancer clinical trials, Oncogene 19 (2000) 6687–6692. https://doi.org/10.1038/sj.onc.1204088.
[16] M.S. Raab, K. Podar, I. Breitkreutz, P.G. Richardson, K.C. Anderson, Multiple myeloma, Lancet 374 (2009) 324–339. https://doi.org/10.1016/s0140-

6736(09)60221-x.
[17] D.J. Kuhn, Q. Chen, P.M. Voorhees, J.S. Strader, K.D. Shenk, C.M. Sun, S.D. Demo, M.K. Bennett, F.W. van Leeuwen, A.A. Chanan-Khan, R.Z. Orlowski, Potent activity of carfilzomib, a novel, irreversible inhibitor of the ubiquitin-proteasome pathway, against preclinical models of multiple myeloma, Blood 110 (2007) 3281–3290. https://doi.org/10.1182/blood-2007-01-065888.
[18] P. Moreau, T. Masszi, N. Grzasko, N.J. Bahlis, M. Hansson, L. Pour, I. Sandhu, P. Ganly, B.W. Baker, S.R. Jackson, A.M. Stoppa, D.R. Simpson, P. Gimsing, A. Palumbo, L. Garderet, M. Cavo, S. Kumar, C. Touzeau, F.K. Buadi, J.P. Laubach, D.T. Berg, J. Lin, A. Di Bacco, A.M. Hui, H. van de Velde, P.G. Richardson PG1, TOURMALINE-MM1 study group. Oral ixazomib, lenalidomide, and dexamethasone for multiple myeloma, N. Engl. J. Med. 374 (2016) 1621–1634. https://doi.org/10.1056/NEJMoa1516282.
[19] L. Borissenko, M. Groll, 20S proteasome and its inhibitors: crystallographic knowledge for drug development, Chem. Rev. 107 (2007) 687–717. https://doi.org/10.1021/cr0502504.
[20] P. Beck, C. Dubiella, M. Groll, Covalent and non-covalent reversible proteasome inhibition, Biol. Chem. 393 (2012) 1101–1120. https://doi.org/10.1515/hsz-2012-0212.
[21] M. Hasegawa, Y. Yasuda, M. Tanaka, K. Nakata, E. Umeda, Y. Wang, C. Watanabe, S. Uetake, T. Kunoh, M. Shionyu, R. Sasaki, I. Shiina, T. Mizukami, A novel tamoxifen derivative, ridaifen-F, is a nonpeptidic small-molecule proteasome inhibitor, Eur. J. Med. Chem. 71 (2014) 290–305. https://doi.org/10.1016/j.ejmech.2013.11.009.
[22] A.D. Frankel, C.O. Pabo, Cellular uptake of the tat protein from human immunodeficiency virus, Cell 55 (1988) 1189–1193. https://dx.doi.org/10.1016/0092-8674(88)90263-2.
[23] S. Reissmann, Cell penetration: scope and limitations by the application of cell-penetrating peptides, J. Pept. Sci. 20 (2014) 760–784. https://doi.org/10.1002/psc.2672.
[24] S. Futaki, T. Suzuki, W. Ohashi, T. Yagami, S. Tanaka, K. Ueda, Y. Sugiura, Arginine-rich peptides. An abundant source of membrane-permeable peptides having potential as carriers for intracellular protein delivery, J. Biol. Chem. 276 (2001) 5836–5840. https://doi.org/10.1074/jbc.M007540200.
[25] L.R. Wright, J.B. Rothbard, P.A. Wender, Guanidinium rich peptide transporters and drug delivery, Curr. Protein Pept. Sci. 4 (2003) 105–124. https://doi.org/10.2174/1389203033487252.
[26] G. Koczan, A.C. Ghose, A. Mookerjee, F. Hudecz, Methotrexate conjugate with branched polypeptide influences Leishmania donovani infection in vitro and in experimental animals, Bioconjugate Chem. 13 (2002) 518–524. https://doi.org/10.1021/bc015530e.
[27] C. Rousselle, P. Clair, J.M. Lefauconnier, M. Kaczorek, J.M. Scherrmann, J. Temsamani, New advances in the transport of doxorubicin through the blood-brain barrier by a peptide vector-mediated strategy, Mol. Pharmacol. 57 (2000) 679–686. https://dx.doi.org/10.1124/mol.57.4.679.
[28] Y. Li, X. Zheng, Z. Cao, W. Xu, J. Zhang, M. Gong, Self-assembled peptide (CADY-1) improved the clinical application of doxorubicin, Int. J. Pharm 434 (2012) 209–214. https://doi.org/10.1016/j.ijpharm.2012.06.003.
[29] P. Zhang, A.G. Cheetham, L.L. Lock, H. Cui, Cellular uptake and cytotoxicity of drug-peptide conjugates regulated by conjugation site, Bioconjugate Chem. 24 (2013) 604–613. https://doi.org/10.1021/bc300585h.
[30] S. Biswas, P.P. Deshpande, F. Perche, N.S. Dodwadkar, S.D. Sane, V.P. Torchilin, Octa-arginine-modified pegylated liposomal doxorubicin: an effective treatment strategy for non-small cell lung cancer, Canc. Lett. 335 (2013) 191–200. https://doi.org/10.1016/j.canlet.2013.02.020.
[31] C. Liu, X.N. Liu, G.L. Wang, Y. Hei, S. Meng, L.F. Yang, L. Yuan, Y. Xie, A dual-mediated liposomal drug delivery system targeting the brain: rational construction, integrity evaluation across the blood-brain barrier, and the transporting mechanism to glioma cells, Int. J. Nanomedicine 12 (2017) 2407–2425. https://doi.org/10.2147/ijn.s131367.
[32] K. Splith, W. Hu, U. Schatzschneider, R. Gust, I. Ott, L.A. Onambele, A. Prokop, I. Neundorf, Protease-activatable organometal-Peptide bioconjugates with enhanced cytotoxicity on cancer cells, Bioconjugate Chem. 21 (2010) 1288–1296. https://doi.org/10.1021/bc100089z.
[33] J. Hoyer, U. Schatzschneider, M. Schulz-Siegmund, I. Neundorf, Dimerization of a cell-penetrating peptide leads to enhanced cellular uptake and drug delivery, Beilstein J. Org. Chem. 8 (2012) 1788–1797. https://doi.org/10.3762/bjoc.8.204.
[34] W. Hu, K. Splith, I. Neundorf, K. Merz, U. Schatzschneider, Influence of the metal center and linker on the intracellular distribution and biological activity of organometal-peptide conjugates, J. Biol. Inorg. Chem. 17 (2012) 175–185. https://doi.org/10.1007/s00775-011-0840-5.
[35] I. Shiina, Y. Sano, K. Nakata, M. Suzuki, T. Yokoyama, A. Sasaki, T. Orikasa, T. Miyamoto, M. Ikekita, Y. Nagahara, Y. Hasome, An expeditious synthesis of tamoxifen, a representative SERM (selective estrogen receptor modulator), via the three-component coupling reaction among aromatic aldehyde, cinnamyltrimethylsilane, and beta-chlorophenetole, Bioorg. Med. Chem. 15 (2007) 7599–7617. https://doi.org/10.1016/j.bmc.2007.09.008.
[36] I. Shiina, Y. Sano, K. Nakata, T. Kikuchi, A. Sasaki, M. Ikekita, Y. Nagahara, Y. Hasome, T. Yamori, K. Yamazaki, Synthesis and pharmacological evaluation of the novel pseudo-symmetrical tamoxifen derivatives as anti-tumor agents, Biochem. Pharmacol. 75 (2008) 1014–1026. https://doi.org/10.1016/j.bcp.2007.11.005.
[37] T. Mukaiyama, Titanium tetrachloride in organic synthesis [new synthetic methods (21)], Angew. Chem. Int. Ed. Engl 16 (1977) 817–826. https://doi.org/10.1002/anie.197708171.
[38] D.D. Yu, B.M. Forman, Simple and efficient production of (Z)-4-hydroxytamoxifen, a potent estrogen receptor modulator, J. Org. Chem. 68 (2003) 9489–9491. https://doi.org/10.1021/jo035164n.
[39] P. Sledz, P. Unverdorben, F. Beck, G. Pfeifer, A. Schweitzer, F. Forster, W. Baumeister, Structure of the 26S proteasome with ATP-gammaS bound provides insights into the mechanism of nucleotide-dependent substrate translocation, Proc. Natl. Acad. Sci. U. S. A. 110 (2013) 7264–7269. https://doi.org/10.1073/pnas.1305782110.
[40] K. Tanaka, T. Yoshimura, A. Ichihara, Role of substrate in reversible activation of proteasomes (multi-protease complexes) by sodium dodecyl sulfate, J. Biochem 106 (1989) 495–500.
[41] A. Kloss, P. Henklein, D. Siele, M. Schmolke, S. Apcher, L. Kuehn, P.W. Sheppard, B. Dahlmann, The cell-penetrating peptide octa-arginine is a potent inhibitor of proteasome activities, Eur. J. Pharm. Biopharm. 72 (2009) 219–225. https://doi.org/10.1016/j.ejpb.2008.10.016.
[42] R.A. Moravec, M.A. O'Brien, W.J. Daily, M.A. Scurria, L. Bernad, T.L. Riss, Cell-based bioluminescent assays for all three proteasome activities in a homogeneous format, Anal. Biochem. 387 (2009) 294–302. https://doi.org/10.1016/j.ab.2009.01.016.
[43] O. Trott, A.J. Olson, AutoDock Vina: improving the speed and accuracy of docking with a new scoring function, efficient optimization, and multithreading, J. Comp. Chem 31 (2010) 455–461. https://doi.org/10.1002/jcc.21334.
[44] J. Schrader, F. Henneberg, R.A. Mata, K. Tittmann, T.R. Schneider, H. Stark, G. Bourenkov, A. Chari, The inhibition mechanism of human 20S proteasomes enables next-generation inhibitor design, Science 353 (2016) 594–598. https://doi.org/10.1126/science.aaf8993.
[45] P. Unverdorben, F. Beck, P. Sledz, A. Schweitzer, G. Pfeifer, J.M. Plitzko, W. Baumeister, F. Forster, Deep classification of a large cryo-EM dataset defines the conformational landscape of the 26S proteasome, Proc. Natl. Acad. Sci. U. S. A. 111 (2014) 5544–5549. https://doi.org/10.1073/pnas.1403409111.
[46] A. Schweitzer, A. Aufderheide, T. Rudack, F. Beck, G. Pfeifer, J.M. Plitzko, E. Sakata, K. Schulten, F. Forster, W. Baumeister, Structure of the human 26S proteasome at a resolution of 3.9 A, Proc. Natl. Acad. Sci. U. S. A. 113 (2016) 7816–7821. https://doi.org/10.1073/pnas.1608050113.
[47] S. Chen, J. Wu, Y. Lu, Y.B. Ma, B.H. Lee, Z. Yu, Q. Ouyang, D.J. Finley, M.W. Kirschner, Y. Mao, Structural basis for dynamic regulation of the human 26S proteasome, Proc. Natl. Acad. Sci. U. S. A. 113 (2016) 12991–12996. https://doi.org/10.1073/pnas.1614614113.
[48] J. Inoue, T. Otsuki, A. Hirasawa, I. Imoto, Y. Matsuo, S. Shimizu, M. Taniwaki, J. Inazawa, Overexpression of PDZK1 within the 1q12-q22 amplicon is likely to be associated with drug-resistance phenotype in multiple myeloma, Am. J. Pathol. 165 (2004) 71–81. https://doi.org/10.1016/S0002-9440(10)63276-2.
[49] M. Kool, M. de Haas, G.L. Scheffer, R.J. Scheper, M.J. van Eijk, J.A. Juijn, F. Baas, P. Borst, Analysis of expression of cMOAT (MRP2), MRP3, MRP4, and MRP5, homologues of the multidrug resistance-associated protein gene (MRP1), in human cancer cell lines, Canc. Res. 57 (1997) 3537–3547.
[50] O. Kocher, N. Comella, A. Gilchrist, R. Pal, K. Tognazzi, L.F. Brown, J.H. Knoll, PDZK1, a novel PDZ domain-containing protein up-regulated in carcinomas and mapped to chromosome 1q21, interacts with cMOAT (MRP2), the multidrug resistance-associated protein, Lab. Invest. 79 (1999) 1161–1170.
[51] E. Ruoslahti, Tumor penetrating peptides for improved drug delivery, Adv. Drug Deliv. Rev. 110–111 (2017) 3–12. https://doi.org/10.1016/j.addr.2016.03.008.
[52] K. Josephson, A. Ricardo, J.W. Szostak, mRNA display: from basic principles to macrocycle drug discovery, Drug Discov. Today 19 (2014) 388–399. https://doi.org/10.1016/j.drudis.2013.10.011.
[53] M. Namba, T. Ohtsuki, M. Mori, A. Togawa, H. Wada, T. Sugihara, Y. Yawata, T. Kimoto, Establishment of five human myeloma cell lines, In Vitro Cell. Dev. Biol. 25 (1989) 723–729.
[54] G.M. Morris, R. Huey, W. Lindstrom, M.F. Sanner, R.K. Belew, D.S. Goodsell, A.J. Olson, AutoDock4 and AutoDockTools4: automated docking with selective receptor flexibility, J. Comp. Chem 30 (2009) 2785–2791. https://doi.org/10.1002/jcc.21256.
[55] M.J. Vainio, M.S. Johnson, Generating conformer ensembles using a multi-objective genetic algorithm, J. Chem. Inf. Model. 47 (2007) 2462–2474. https://doi.org/10.1021/ci6005646.
[56] E.F. Pettersen, T.D. Goddard, C.C. Huang, G.S. Couch, D.M. Greenblatt, E.C. Meng, T.E. Ferrin, UCSF Chimera–a visualization system for exploratory research and analysis, J. Comp. Chem 25 (2004) 1605–1612. https://doi.org/10.1002/jcc.20084.